

N O T I C E

THIS DOCUMENT HAS BEEN REPRODUCED FROM
MICROFICHE. ALTHOUGH IT IS RECOGNIZED THAT
CERTAIN PORTIONS ARE ILLEGIBLE, IT IS BEING RELEASED
IN THE INTEREST OF MAKING AVAILABLE AS MUCH
INFORMATION AS POSSIBLE

**NASA CR-159739
EDR 10085**

PLASMA-SPRAYED DUAL DENSITY CERAMIC TURBINE SEAL SYSTEM

(NASA-CR-159739) PLASMA-SPRAYED DUAL
DENSITY CERAMIC TURBINE SEAL SYSTEM Final
Report (Detroit Diesel Allison,
Indianapolis, Ind.) 67 p HC A04/MF A01

N80-15411

Unclas
CSCL 11A G3/37 46585

FINAL REPORT

By

D.L. Clingman, B. Schechter, K.R. Cross, J.R. Cavanagh

**DETROIT DIESEL ALLISON
DIVISION GENERAL MOTORS CORPORATION
INDIANAPOLIS, INDIANA 46206**

**Prepared For
NATIONAL AERONAUTICS AND SPACE ADMINISTRATION**

OCTOBER 1979

**NASA LEWIS RESEARCH CENTER
CONTRACT: NAS 3-21263**



1. Report No. NASA CR-159739		2. Government Accession No.		3. Recipient's Catalog No.	
4. Title and Subtitle Plasma-Sprayed Dual Density Ceramic Turbine Seal System				5. Report Date October 1979	
				6. Performing Organization Code	
7. Author(s) D. L. Clingman; B. Schechter; K. R. Cross; J. R. Cavanagh				8. Performing Organization Report No. EDR 10085	
				10. Work Unit No.	
9. Performing Organization Name and Address Detroit Diesel Allison Division General Motors Corporation Indianapolis, Indiana				11. Contract or Grant No. NAS3-21263	
				13. Type of Report and Period Covered Contractor Report	
12. Sponsoring Agency Name and Address Propulsion Laboratory U. S. Army R&T Labs (AVRADCOM) Lewis Research Center Cleveland, Ohio 44135				14. Sponsoring Agency Code	
15. Supplementary Notes Final Report. Project Manager, R. C. Bill, Fluid System Components Division, NASA Lewis Research Center Cleveland, Ohio					
16. Abstract Dual density plasma-sprayed ceramic coating systems were investigated for possible application as abradable turbine tip seal systems in small gas turbine engines typical of the Army Advanced Technology Demonstrator Engine (ATDE). Abradability, erosion resistance, internal leakage, and microstructural characterization were investigated for polyester- and cenosphere-filled zirconium oxide composites. Results indicate the polyester system is more abradable but displays significantly less erosion resistance than the cenosphere system. The absence of significant blade tip damage during abradability testing of both systems suggests that additional effort may result in a more nearly optimum balance of abradability and erosion resistance.					
17. Key Words (Suggested by Author(s)) Abradable seals Zirconia High temperature seals Plasma-sprayed Turbine seals Porous Gas path seals Ceramic seals				18. Distribution Statement Unclassified Unlimited	
19. Security Classif. (of this report) Unclassified		20. Security Classif. (of this page) Unclassified		21. No. of Pages	
				22. Price*	

* For sale by the National Technical Information Service, Springfield, Virginia 22161

FOREWORD

This Final Technical Report covers the work performed by the Materials Research and Engineering group, Detroit Diesel Allison Division, General Motors Corporation under NASA Contract NAS 3-21263. The NASA Project Manager was Dr. R. C. Bill of the NASA Lewis Research Center.

PRECEDING PAGE BLANK NOT FILMED

TABLE OF CONTENTS

	<u>Page</u>
Abstract	i
Foreword	iii
List of Illustrations	vi
List of Tables	ix
Summary	1
Introduction	2
Seal System Development	3
Test Apparatus	8
Test Results	10
Discussion of Results	14
Conclusions	15

PRECEDING PAGE BLANK NOT FILMED

LIST OF ILLUSTRATIONS

<u>Figure</u>		<u>Page</u>
1	Cross Sections of Thermal Barrier Coating Configurations	21
2	High Speed/High-Temperature Abradable Seal Materials Test Rig	22
3	Erosion Test Rig	23
4	Standard Density Zirconia Erosion - 90° Impingement	24
5	Standard Density Zirconia Erosion - 45° Impingement	25
6	Standard Density Zirconia Erosion - 15° Impingement	26
7	Permeability Test Device	27
8	System I-P Abradability - Slow Incursion Rate	28
9	System II-P Abradability - Slow Incursion Rate	29
10	System III-P Abradability - Slow Incursion Rate	30
11	System I-P Abradability - Fast Incursion Rate	31
12	System II-P Abradability - Fast Incursion Rate	32
13	System III-P Abradability - Fast Incursion Rate	33
14	System I-P Erosion	34
15	System II-P Erosion	36
16	System III-P Erosion	38
17	Erosion of Polyester and Cenosphere Zirconia Systems	40
18	Abradable Seal Material Permeability	41
19	System I-C Abradability - Slow Incursion Rate	42
20	System II-C Abradability - Slow Incursion Rate	43
21	System III-C Abradability - Slow Incursion Rate	44
22	System I-C Erosion	45
23	System II-C Erosion	46
24	System III-C Erosion	49
25	System I-P Microstructure	51
26	System II-P Microstructure	52

LIST OF ILLUSTRATIONS (Continued)

<u>Figure</u>		<u>Page</u>
27	System III-P Microstructure	53
28	System II-P Line Scan Analysis	54
29	System II-P Element Mapping	55
30	System I-C Microstructure	56
31	System II-C Microstructure	57
32	System III-C Microstructure	58
33	System I-C Line Scan Analysis	59
34	System II-C Line Scan Analysis	60

LIST OF TABLES

<u>Table</u>		<u>Page</u>
I	Plasma Spray Parameters	16
II	Surface Roughness Measurements	17
III	Coating System Hardness	18
IV	Coating System Composition	19
V	Summary of Abradability Tests	20

SUMMARY

The objective of this program was to develop a plasma-sprayed dual density ceramic abradable seal system for direct application to the HPT seal shroud of small gas turbine engines. The system concept is based on a moderately high density ceramic layer adjacent to the metal shroud to provide thermal-stress cushioning for the abradable outer layer, consisting of a specially formulated reduced-density ceramic.

The program scope consisted of three iterations on each of two different coating systems. The investigations included coating processes, abradability, erosion resistance, permeability, and microstructural characterization.

Results obtained with the polyester-filled system showed excellent abradability but relatively poor erosion resistance characteristics. The cenosphere-filled system produced somewhat less-impressive abradability characteristics but was much more erosion resistant than the polyester system. Blade tip distress was not considered excessive for either system.

Both systems require additional effort to optimize the balance between abradability and erosion resistance before commitment to engine evaluation can be made.

INTRODUCTION

Efficiency of small gas turbine engines in the size class of the Army's 800 shp Advanced Technology Demonstrator Engine (ATDE) is extremely sensitive to operating clearances between compressor and turbine blade tips and the stationary seal components. From the standpoint of specific fuel consumption (SFC) the single most significant blade tip clearance location is the high pressure turbine (HPT). The plasma-sprayed ceramic seal system investigated in this program was prompted by the lack of a satisfactory available seal system adaptable to the HPT application.

Two different, yet similar, concepts were selected for development, each incorporating a dual density plasma-sprayed ceramic system to be applied directly to the HPT seal shroud. Both systems employ a moderately high density ceramic layer of approximately 12% porosity adjacent to the metal shroud substrate and metallic bond coat to mitigate the mismatch in thermal expansion characteristics between the metallic and low density ceramic components of the system. The low density ceramic outermost layer of the system provides abrasability.

The two systems selected for development differ only in the approach taken in improving the abrasability of the outer layer. One system uses a sacrificial filler to produce the desired density reduction through controlled porosity brought about by thermal decomposition of the filler. The second approach employs a temperature-resistant low density filler which is distributed throughout the abrasable layer and remains intact following exposure to elevated temperature.

SEAL SYSTEM DEVELOPMENT

The seal systems developed during this program have built upon the ever-increasing background of success obtained with the NASA-developed yttria-stabilized zirconia (YSZ) thermal barrier coating systems. The basic philosophy guiding the program has been to start with a proven high temperature material, preferably one with significant engine experience, and to modify the coating structure toward the end of improving the abrasability of the material while retaining the desirable high temperature characteristics of the original coating system. The end result becomes an "abrasable thermal barrier".

Coating Configuration

Typically, the NASA coating successes have been achieved with "thin" coating systems--i.e., bond coats 0.013-0.018 cm (0.005-0.007 in.) and oxide layers 0.038-0.051 cm (0.015-0.020 in.) thick, as shown in Figure 1a. Further, the coatings have been "duplex" in that only two discrete layers are present, with no "graded" or mixed-composition layers.

From the structure of the dual-density coating system, shown in Figure 1b, it is readily apparent that the concept involves essentially the addition of a 0.046-0.051 cm (0.018-0.020 in.) reduced-density abrasable layer superposed on top of the basic NASA thermal barrier coating. An incursion of turbine blades into a rub track, particularly in small engines such as the GMA 500/ATDE, is unlikely to exceed 0.025-0.038 cm (0.010-0.015 in.) without considerable damage being incurred by the rotor system. The coating system geometry selected has provided for this margin in the abrasable outer layer.

Specimen Fabrication

The basic concept of an abrasable thermal barrier depends on devising a method whereby the density in the blade track region of the seal is reduced below that normally obtained in the plasma-spray process. One attractive method for accomplishing the desired density reduction is to "co-spray" a sacrificial "filler" concurrently with the YSZ of the thermal barrier. This procedure interrupts the continuity of the YSZ and is followed by thermal decomposition of the filler to produce a controlled level of porosity. A major difficulty in using this technique arises from the significantly different temperature capabilities (melting points) of YSZ and candidate fillers. It is this feature that prevents the constituent powders from being bound together and sprayed as a single composite material, since particle temperatures adequate for softening YSZ (required for good deposition) would surely result in premature decomposition of the filler.

A workable solution to the problem of spraying materials with such vastly different characteristics has resulted from providing different residence times in the plasma stream for each constituent powder according to its particular requirements. This is accomplished by introducing the high-temperature component (YSZ) through a powder feed port directly into the plasma-spray gun body. The low-temperature component (polyester) is fed by a separate powder feeder into the plasma stream external to the gun body at a point downstream from the nozzle. The polyester filler currently used in preparing specimens of one system for this program is subsequently

thermally decomposed by heating in air at 982°C (1800°F) for a period of 4 hours. This non-optimized heat treatment has proven to be adequate for removing the filler constituent. However, no attempt has been made to determine whether lower temperatures and/or lesser times would also suffice.

Fabrication Equipment

The plasma spray equipment used in constructing the various coating specimens was identical to that used by NASA in developing the yttria-stabilized zirconia thermal barrier coating system. The Plasmadyne Model SG-1B plasma-spray gun used exclusively for deposition of all layers of the coatings has powder feed ports located both internal and external to the gun body. Normally, only one of these ports is used at a time. However, because of the peculiar requirements of the filled coating layer, separate Plasmadyne Model 1000-A powder feeders are used to supply both ports simultaneously - the YSZ being introduced within the gun body and the filler powder injected into the plasma stream through the external downstream port. With this arrangement the optimum parameter ranges for the multiple component system reflect a compromise of the requirements of the individual component powders.

Filler Constituents

Polyester-Filled Systems

The sacrificial "filler" powder used to create the controlled porosity in the abrasible layer of the I-P, II-P, and III-P systems was Metco 600, a commercially available polyester powder suitable for plasma spray applications. Additional characterization of this powder beyond that provided by the manufacturer was limited by the tendency of the powder to adhere to the walls and screens of the various sieves during attempts to document particle size distributions. Thermally, the powder was found to char at a temperature of approximately 552°C (1025°F) which is appreciably below the 982°C (1800°F) temperature selected for thermal decomposition.

Cenosphere-Filled Systems

Alumino-silicate spheres ("cenospheres") comprise the "filler" used to improve the abrasibility of the outer layer of the I-C, II-C, and III-C systems. This material, which was supplied for the program investigations by NASA is essentially "fly-ash", a pollution by-product derived from the electric power generating industry. Low density, hollow cenospheres are reported to be selectively separated from solid spheres by a flotation process in which the heavier solid particles sink to the bottom of the container. The buoyant hollow spheres are skimmed from the surface of the liquid and dried prior to subsequent use.

Sieve analysis of the cenospheres was inconclusive, as in the case of the polyester powder. The particles displayed a pronounced tendency to adhere to the screens and walls of the sieves, probably as a result of static electrical charging of the particles. However, under optical examination at 30X magnification, an extremely broad particle size distribution was observed. No attempt was made to reduce the range of particle sizes since no difficulty was encountered in spraying the material in the as-received condition.

Processing Procedures

All substrate materials used in this investigation were Hastelloy X. This is the same material as that used for the shroud segments of the GMA 500/ATDE and ensures that a fully developed coating system will be compatible with engine hardware.

The elapsed time between plasma spray processing steps was held to the minimum possible consistent with exercising care and good technique, and in no case was allowed to exceed 2 hours. This condition thus required that all specimens be completed the same day that they were started.

Prior to deposition of each particular coating system, the substrates were prepared by vapor degreasing, followed by grit blasting with 60 grit aluminum oxide. Because of the number of specimens (12) prepared for each iteration, fabrication was accomplished in two batches of six specimens each.

Powder flow rates were precisely determined by collecting and weighing timed specimens of material delivered by the powder feeder. Spray distances were the same as those established by NASA for the several discrete layers of the coatings, with the same distance maintained for both the standard density layers and the filled layers, regardless of the filler employed. All spraying was done with hand-held equipment, specimens oriented vertically, and cooling air supplied to the rear face of the specimen coupons. Deposit efficiency appeared to play a significant role in the preparation of the cenosphere-filled coatings, since little variation in attainable composition was achieved.

Bond Coat Powder

The bond coat employed in all instances was NiCrAlY obtained from Alloy Metals, Inc., Troy, Michigan, with the following chemical composition:

Cr 16.2%
Al 5.5%
Y 0.6%
Ni Balance

Mesh specification was -200 +325. The material was identical to that developed for the NASA thermal barrier coating, including the source of supply. A 13.6 kg (30 lb.) developmental heat of the material yielded a net of 12.3 kg (27 lbs) of which only 2.3 Kg (5 lbs) was within the -200 +325 mesh required for plasma spraying. The remaining material was nearly equally divided between +200 and -325 mesh sizes, neither of which was found to feed or spray satisfactorily.

Oxide Layer Powder

The yttria-stabilized zirconia powder employed in this investigation marked a potentially significant departure from the NASA-developed thermal barrier materials. Because the material used in the NASA-developed coatings was quite expensive and had a history of lengthy delivery times, M. tco 202-NS was selected for the oxide layer component in the interest of controlling costs

and expediting the execution of the program. The principal difference between the two powders is in the method of stabilization. Metco 202-NS achieves stabilization during the spray process instead of by pre-alloying and is available off the shelf at a fraction of the cost of the pre-stabilized material.

Recent, and as yet unpublished, investigations at DDA on various combinations of bond coat and yttria-stabilized zirconia materials indicates that the NASA-developed material possesses superior thermal shock/fatigue resistance compared to other materials tested. Should this factor eventually prove troublesome with the dual-density systems under development, a minimum of effort is expected in order to effect a material change if required.

Standard Density Layers

Parameters and techniques identical to those used by NASA were employed in depositing the standard density intermediate layer for each coating configuration. As previously mentioned, however, Metco 202-NS was substituted for the pre-alloyed yttria-stabilized zirconia used in the NASA-developed thermal barrier coatings.

Abradable Layers

The most significant parameter to evolve in the preparation of abradable layers, regardless of the "filler" employed, was the ratio of zirconia to filler material. Since the deposit efficiencies of the materials generally differ, the starting ratios were likewise different from the ratios in the deposited coating.

Some modification of the standard density layer parameters was required to optimize the deposition of the high melting point zirconia without incurring premature softening or melting in the filler materials. Even though the filler powders were introduced into the plasma stream through an external feed port, a significant reduction in both arc current (-20%) and operating voltage (up to -10%) were required. These parameter variations were initially established for the polyester-filled system and carried through for the cenosphere filled-system without any further changes. The spray parameters for each of the coating systems are listed in Table I.

Surface Machining

The surface of each specimen was prepared by machining with a single-point cutting tool of the replaceable carbide insert variety prior to any further conditioning (e.g., burn-out in the case of polyester-filled coatings).

Machining parameters were determined for the I-P coating system by trial and error using both single-point machining and wet grinding techniques. The coating was found to machine easily with either method, and as expected, the smoother surface was obtained by grinding. Specimens subjected to the grinding operation were flushed with clear water and dried in vacuum to remove any contamination from the grinding coolant. The parameters established for the I-P system were used for the machining of all subsequent coating systems. These parameters were:

- o Cutting tool Carbide Insert - TPG 431-KG8
- o Work Speed 118.9 cm/min (390 ft/min)
- o Cross Feed 0.015 cm/min (0.006 in/min)
- o Material removed per pass 0.025 cm (0.010 inches)

Roughness measurements were made prior to thermal decomposition of the polyester filler for the I-P system. These measurements included readings for both a ground as well as a machined surface. The order of magnitude of attainable surface finish for the I-P system represents an upper bound when compared to high density coating systems as can be seen from Table II. This table is a compilation of the surface roughness of each of the coating systems as taken after surface machining.

Hardness of the I-P coating system was measured for the as-sprayed and machined configurations, both before and after thermal decomposition of the polyester filler. The R15Y superficial hardness scale (15 kg load, 1.27 cm ($\frac{1}{2}$ inch) diameter ball indenter) was found to be satisfactory for the softer coatings typified by the I-P system, but lacked sufficient definition for the harder coatings. Consequently, some of the harder coating systems necessitated use of the R15W scale (15 kg load 0.32 cm ($\frac{1}{8}$ inch) diameter indenter) as an alternate measurement system. Measurements obtained from both systems are provided in Table III.

TEST APPARATUS

High Speed Abradability Rig

The abradability evaluations were conducted on the high speed, high temperature test rig shown in Figure 2. This rig consists of a steam turbine-driven spindle with replaceable test disks. The program test condition of 228.6 m/sec (750 ft/sec) requires the unit to rotate at 29,650 rpm, approximately one-half the design limit.

The heat source for this test unit is a quartz lamp furnace which is limited to 760°C (1400°F) due to mechanical design constraints of the disk/shaft attachment. Evaluation temperatures of 538°C (1000°F) were specified for this program. This temperature was achieved during rig warmup at 5000 rpm but could not be maintained at levels greater than 302°C (575°F) when the disk was brought to operating speed because of cooling resulting from excessive windage in the furnace cavity.

The mechanism used to provide the rub incursion motion is designed around a rigid frame system which supports the test coupon above the rotating IN 792 test disc in the quartz lamp heated cavity. The vertical incursion drive is fixed to the frame above the test coupon through a thin flexure which essentially isolates the normal and tangential forces produced by the rub. The rub interaction rates of 0.0025 cm/sec (0.001 in/sec) and 0.025 cm/sec (0.010 in/sec) are achieved by controlling the pulse rate of a stepping motor which drives a lead screw. Normal force signals are sensed by a load cell positioned between the lead screw and the flexure leaf. The tangential force signals are transmitted by a rigid load frame through swivel couplings to two load cells mounted outside the heated cavity. The tangential force signals are then summed electrically to provide the instantaneous tangential force signal.

Erosion Test Rig

Erosion tests were conducted on the apparatus shown in Figure 3. The specimen is mounted at the prescribed angle to the impinging air/particulate stream. The tests were performed at room temperature with the particulate flow rate set at a nominal 20 gms/hr (0.044 lb/hr) and the air flow nominally at 11.2 m³/hr (400 ft³/hr) with a supply pressure of 482.3 KPag (70 psig). A timer shuts the rig off at the predetermined time. The erosive medium used was AC Coarse Air Cleaner Dust (Natural Arizona Road Dust) which is primarily calcium silicate and has the following particle size distribution:

0.5 microns	12%
5-10 microns	12%
10-20 microns	14%
20-40 microns	23%
40-80 microns	30%
80-200 microns	9%

Specimen and dust reservoir weights are recorded prior to and at the conclusion of each test.

The angular incidence of the specimen with respect to the erosive air stream was selected as 15° based on the tests of the standard density system shown in Figures 4 through 6. The 15° setting, Figure 6, was considered to be most representative of engine air flow conditions and would not unduly penalize candidate coating systems.

Permeability Rig

Through-leakage as a result of interconnected porosity is evaluated on the rig schematically shown in Figure 7. This simple fixture consists essentially of inlet and exhaust ports which are formed in a polyurethane insert in the cover. When the cover is clamped in place over the sample, the polyurethane acts as a seal preventing leakage across the abradable surface to the exhaust port or to the atmosphere. The incoming argon is thereby forced to pass through the abradable material in order to reach the exhaust port. The feed port is connected to a pressure gage, flowmeter and argon tank and the exhaust port is open to the atmosphere. Pressure is set at the argon tank by means of a regulator, and through-flow in the coating is monitored at the flowmeter. The area used for the flow calculation is the actual cross sectional area of the specimen.

TEST RESULTS

Polyester-Filled Systems

Abradability

Abradability test results of the polyester filled systems are illustrated in Figures 8-13.

The I-P polyester-filled system is shown in Figure 8 for the slow incursion rate of 0.0025 cm/sec. (0.001 in/sec.) The absence of transferred metal from the blade tip to rub track illustrates the fine abrasability characteristics of this material. The blade tip showed no evidence of distress or loss of material. A slight burnishing was present as can be seen by the faint discoloration of the tips in Figure 8. Depth of the rub was 0.013 cm (0.005 in.).

The II-P polyester system slow incursion rate rub is shown in Figure 9. The rub path produced by the rotating blade tips shows no evidence of metal transfer or tendency towards glazing. Depth of the rub was 0.038 cm (0.015 in.). The blade tip showed no evidence of the rub. Measured tip loss was 0.00051 cm (0.0002 in.) which is discounted as being within measurement tolerance.

Figure 10 shows the slow incursion rate abrasability results for the III-P materials system. This was a well-defined clean rub trace with no evidence of glazing or transferred metal on the surface of the abrasable material. The blade tip condition was excellent with no evidence of any distress present. No loss of blade tip material could be measured. The depth of rub was 0.038 cm (0.015 in.).

Figure 11 was the result of the fast incursion rate rub for the I-P material system. During the course of this test, the penetration depth of the blade tip exceeded the depth of the outer abrasable layer and came into contact with the more dense YSZ sub-layer. The result was a two-phase rub. Close examination of the rub track showed that the glazed area was initiated at 0.043 cm (0.017 in.) below the surface of the coating, which is the thickness of the abrasable top layer. Total rub depth was 0.053 cm (0.021 in.). The blade tips show definite evidence of a rub, as can be seen in Figure 11; however, no severe distress is present. The apparent damage seen in Figure 11 is more of a burnishing which produces a series of color variations on the tip of the blade rather than a physical scoring or galling of the surface. This scoring or galling of the surface is commonly present in most all-metal abrasable systems. Measured blade tip loss was of the order of 0.00051 cm (0.002 in.).

The result of the fast incursion rate abrasability test with the II-P material system is shown in Figure 12. Glazing of the material occurred almost immediately upon contact, accompanied by thermal cracking at the surface of the rub path and some particle pullout. No metal debris could be seen in the rub track. The blade tip shows severe burnishing and visual indications of streaking, but there was little evidence of any physical scoring or galling taking place. The measured rub depth was 0.013 cm (0.005 in.) and the maximum blade tip loss was .0015 cm (.0006 in.).

Figure 13 shows the condition of the rub track and the blade tips for the fast incursion rate with the III-P materials system. The rub track was very clean and distinct except for a slight amount of metal pickup at one edge of the rub path. The blade tip shows no evidence of distress and no burnishing is present. The maximum amount of blade tip loss was 0.0025 cm (0.001 in.) and the depth of penetration in the abradable layer was 0.041 cm (0.016 in.).

Erosion Resistance

Erosion tests were performed on each of the sample systems in accordance with the test description and apparatus previously described. A particularly unusual phenomenon occurred with the I-P system which can be observed in Figures 18 a through d. A layering of the coating took place during fabrication and was immediately observed after machining the samples, Figure 14a. This layering could also be observed in the erosive patterns produced, as seen in Figures 14 b, c, d. This did not occur in any of the other systems and is believed to be an inconsistency in the plasma spray process, possibly resulting from spray technique employed in fabricating early specimens. It is also noted that the I-P system experienced the most severe total erosion damage of all the systems as well as the highest rate of damage. In the first 30 minute period, the sample was virtually eroded away to the more dense YSZ sub-layer. Erosion of the II-P coating system is shown in Figures 15a through d. The layering observed in the I-P coating, Figure 14a, was not present in the II-P coating, Figure 15a. Improved erosion resistance of the II-P coating over the I-P system can be observed as early as the completion of the 30 minute test (Figures 15b compared to Figure 14b). Erosion of the III-P coating system, shown in Figures 16a through d, behaved similar to the I-P system. The specific erosion resistance plotted as a function of time is shown for all the systems in Figure 17.

Permeability

Gas flow permeability for each polyester-filled coating system was checked in accordance with the procedure previously described. Static input pressures up to 344.5 KPag (50 psig) were applied with zero leakage noted. These results are compared with the results obtained for conventional abradable materials in Figure 18.

Cenosphere - Filled Systems

Abradability

Figures 19 through 21 are the results of the slow incursion rate abrasability tests on the cenosphere-filled coating systems. These coatings were generally characterized by a very audible telegraphing of the rotating blade tip contacting the abradable surface. The presence of severe glazing and thermal cracking in the surface of the abradable layer during the slow incursion rate tests suggested a more rapid incursion rate could result in possible damage to the test rig and were therefore deleted from the test program. In all instances, the wear scar appeared to be glassy in nature and layered above the surface of the wear path. The layering appears to start at the entrance to the rub zone and builds in thickness as the blade path exits the material. The blade tips all exhibit heavy burnishing and some scoring and it is likely that some glazed material adhered to the blade tips, thereby preventing an accurate measure of blade tip loss. This loss as best determined,

measured 0.0025 cm (0.001 in.) on the I-C test, 0.00051 cm (0.0002 in.) on the II-C test and 0.00015 cm (0.0006 in.) on the III-C test. Depth of rub was 0.013 cm (0.005 in.), 0.031 cm (0.012 in.) and 0.023 cm (0.009 in.) for the I-C, II-C, and III-C tests respectively.

Erosion Resistance

Erosion test results of the cenosphere-filled systems are shown in Figures 22 through 24. No evidence of layering, as was observed in the I-P system, was present in any of the cenosphere-filled coatings. Erosion resistance of the cenosphere-filled systems was significantly improved over the polyester-filled systems. The specific erosion resistances, as plotted in Figure 17, of the three cenosphere filled systems were very similar in erosive performance, as could be expected when comparing the final composition listed in Table IV.

Permeability

Permeability for each coating was checked to 344.5 KPag (50 psig) with zero leakage noted. Both polyester- and cenosphere-filled systems displayed superior leakage characteristics in comparison with more common abradable materials, as shown in Figure 18.

Microstructure Determination Polyester-Filled Systems

Porosity Level

The porosity level of the specimens I-P, II-P, and III-P were measured and tabulated in Table IV. Section views of the I-P, II-P, and III-P coatings (100X) are displayed in Figure 25a, Figure 26a, and Figure 27a. The progression of the iterations I-P, II-P and III-P leading to lower porosity levels shows that both the pore size and pore distribution decreased in subsequent iterations. It may be noted that the thickness of the porous oxide layer, as shown in Figure 25a, is inconsistent with the thickness shown in Figure 1b. This resulted from sectioning the coating at the end of the specimen, where the outer layer spray pattern tapered slightly toward the substrate.

Ceramic Particles Morphology

Cross-section views at 1000X of I-P, II-P, and III-P are shown in Figure 25b, Figure 26b, and Figure 27b. The views shown display the coating fine structure resulting from plasma spray co-deposition of the polyester and YSZ powders followed by the burn-out of the polyester phase. The level of polyester powder in the plasma spray operation affects the coating structure. Particles of polyester are trapped to form voids and provide a foreign material to weaken the mechanical bonding between the deposited ceramic YSZ particles. Figure 25b, showing the porous oxide layer of specimen series I-P, shows evidence of a spongy area surrounding some of the YSZ particles which likely lessens the inter-particle bond strength.

Interconnectivity of Coating Pores

A specimen from series II-P was examined by Scanning Electron Microscopy (SEM) at 200X. Figure 28 discloses that the voids resulting from the polyester deposition and burn-out are only randomly connected and rarely

communicate between pores over a path exceeding .013-.020 cm (.005-.008 inches). The "closed pore" structure therefore explains the low permeability of the polyester/YSZ coating series compared to the leaky characteristics of abradable materials such as the sintered metal type of coating structure.

Additionally, Figure 28a and b displays the level of Zr and Y as the sensor traverses over the surface and void areas. The straight line across each view defines the line being scanned for the given element. A minimum level for Zr and Y is indicated as the scan progresses over the void areas.

Figure 29 displays the results of an X-ray analysis of elemental distribution on the surface of the cross section of a II-P specimen. Zone 1 is shown to be a void or surface hole. Zone 2 shows the polished YSZ surface with a major indication for zirconium and a minor indication for yttrium. Minor traces of calcium, silicon and sodium were also noted.

Microstructure Determination Cenosphere-Filled Systems

Porosity Level

The porosity level of the test specimen series I-C, II-C, and III-C is achieved by the in-situ trapping of the hollow cenospheres during plasma spray co-deposition with the YSZ ceramic material. Section views of specimens from the series in I-C, II-C and III-C coatings are displayed in Figure 30a, Figure 31a, and Figure 32a. The progression of the iterations of the I-C, II-C and III-C series was to increase the cenosphere percentage with a goal of improving abrasability. The level of cenosphere entrapment was measured by a point-count technique and found to be 30, 35 and 32 volume percent respectively for I-C, II-C, and III-C as shown in Table IV.

Cenosphere/YSZ Particle Morphology

Cross-section views at 100X of series I-C, II-C, and III-C are shown in Figure 30b, Figure 31b, and Figure 32b. The high magnification reveals that the yttria-stabilized zirconia coating matrix encloses both identifiable whole cenosphere particles and solidified agglomerates of the cenosphere material. The solidified agglomerates appear as fairly smooth glassy type particles with little evidence of fracture through the phase. In contrast, the zirconia matrix exhibits both irregular voids and crack or internal fracture patterns.

Figure 33 illustrates the same I-C series coating at 200X magnification with elemental line scans for zirconium and yttrium identifying the yttria stabilized zirconia (YSZ) zones. The dark grey cenosphere particles and solidified agglomerate zones are indicated by noting the areas where the zirconium line scan is at the minimum level.

A view of the II-C series coating at 200X magnification is presented in Figure 34 with the accompanying elemental line scans again shown for zirconium and yttrium. The II-C SEM micrographs (Figure 31) reveal the zirconia matrix as slightly more spongy in appearance. The size distribution of the cenosphere balls and the solid cenosphere material distributed within the coatings are likely related to the distribution of cenosphere particle size supplied to the plasma spray gun.

DISCUSSION OF RESULTS

The slow incursion rate abrasability tests on the polyester-filled systems display very similar wear scar characteristics. The striking dissimilarity between the three coatings in this matrix is the variation in apparent density between I-P, II-P and III-P as seen in Figures 25, 26 and 27. The intent of the variation in coating system composition was to decrease the polyester content as the testing progressed in order to produce an abrasable system which also possessed the desired erosion resistance characteristics.

The IP coating system was targeted for a volume ratio of 65% ZrO_2 and 35% polyester. The actual measured results were 72% and 28%, respectively. The IIP coating was designed to nominally increase the ZrO_2 density of the coating by 10% over the IP system. The measured result was 79% dense instead of the targeted 75%. The resultant hardness, abrasability and erosion tests results support the observed increase in density. The hardness increased from 13 to 89 on the RL5Y scale. The specific erosion decreased as expected and the fast incursion rate abrasability test resulted in a glazed track which occurred solely in the porous top layer. In the I-P test, the glazed track did not appear until the blade tip passed through the abrasable layer and came into contact with the subsurface standard density layer. It was observed that the I-P system was so soft that the porous surface layer was eroded during the first 30 minutes of testing. Subsequently, the erosion was presumably taking place in the standard density layer, which naturally offered much more resistance. This accounts for the wide variation in slope between 30 and 60 minutes for the I-P test.

The III-P system which, although more dense than the II-P system exhibited some of the performance characteristics of a softer coating. The 100X micrographs indicate the density of the porous oxide layer is increasing as intended, from I-P to II-P to III-P. However, the hardness decreased substantially from II-P to III-P and the specific erosion resistance of III-P was very similar to that of I-P. The forces encountered during the slow incursion rate rubs support the oxide layer composition analysis. That is, the normal and tangential forces increase in value with increasing density for this series of runs. However, for the fast incursion rate tests, the normal forces follow the glazing trend. For example, the II-P-F run, which had a glazed rub, also had a high value for the normal load. Glazing in the I-P-F run is discounted due to the blade tip striking the standard density layer. Normal loads were not recorded for the I-P-F run due to an instrumentation failure.

The desired increase in density for the polyester-filled system was nominally achieved through variation of the polyester content during spraying. Projected increases in coating density were achieved by this method and proportionate increases in hardness and erosion resistance occurred for the II-P system, when compared to the I-P coating. However, the III-P system, although more dense than either the I-P or II-P coating systems, did not reflect the increased density in the hardness survey or in the erosion test. This paradox has not been satisfactorily explained. Abrasability tests at slow incursion rates did not result in any discernable differences in the rub paths; fast incursion rates produced observable variations as noted above.

Compositional changes in the cenosphere-filled system to provide for a more abrasable coating were not as pronounced as expected. The desired cenosphere percentages were never achieved and only nominal differences were

observed in the erosion test results. However, these coatings all resulted in significantly better erosion resistance than any of the polyester-filled systems. The normal forces registered during the rubs of the cenosphere filled system were appreciably lower than the glaze-producing normal forces encountered for the polyester systems. No explanation has been found for the inability to achieve the desired porosity level. Since the coatings deposited readily, the explanation may be related to the particle size distribution of the cenospheres.

Additional studies could prove beneficial for the continued development of the cenosphere system. It was noted that the cenosphere particles had a wide variation in size. This may have resulted in poor reproducibility of the coating as well as the inability to effectively control the density of the top layer. In addition, a large proportion of the smaller particles appeared to be solid in nature which could result in an extremely closely-packed structure and contribute to the formation of the glassy phase observed in some of the cenosphere tests. Future effort should therefore include:

- O More effective particle screening. This would reduce the cenosphere particle size distribution to one more appropriate for plasma spray operations.
- O Removal of solid cenosphere particles. This would enhance the resultant abrasible structure and tend to reduce the tendency towards smearing.
- O Investigation of additional filler materials other than the cenospheres. Further work with the polyester filler is not strongly recommended.

CONCLUSION:

The application of a sacrificial filler material to provide controlled or predictable porosity in a ceramic abrasible seal system offers some degree of promise. The use of a co-sprayed polyester filler material did indeed provide an impermeable, porous structure which was readily abrasible. However, erosion resistance was notably lacking. Attempts to improve the erosion performance while still maintaining adequate abrasibility were only marginally successful in that although densities were measurably increased by 15%, hardness and erosion resistance were unpredictable. Co-spraying of a cenosphere-filled system did provide acceptable erosion resistance but abrasibility performance did not appear to be as good as for the polyester-filled systems. A glazed wear scar appeared to be a prominent feature of each of the cenosphere-filled iterations. Attempts to decrease the density of the abrasible layer by increasing the percentage of cenospheres in the coating did not appear to be effective. Blade tip measurements made on both the polyester and cenosphere systems indicate a lower tip loss was recorded for the cenosphere-filled than for the polyester-filled system. At present, the effect of the presence of the glazed wear scar in an actual engine configuration is unknown, particularly when successive blade tip contacts are made.

Results of the through flow leakage, or permeability tests indicate no significant leakage was present for either of the systems in any of the iterations.

Conting System Parameter	<u>I-P</u>	<u>II-P</u>	<u>III-P</u>	<u>I-C</u>	<u>II-C</u>	<u>III-C</u>
Operating Voltage	32	32	32	32	30	30
Current-Amps	450	450	450	450	450	450
Primary Arc Gas	AR	AR	AR	AR	AR	AR
CFH	60	60	60	60	60	60
Line Pressure psig	50	50	50	50	50	50
Feeder Carrier Gas	AR	AR	AR	AR	AR	AR
CFH: Filler/YSZ	12/10	12/10	12/10	12/12	12/12	12/12
Line Pressure psig	50	50	50	50	50	50
Feeder Pot. Setting Filler /YSZ	15/30	13/35	15/55	30/30	36/24	40/20
Spray Distance Cm. Inches	7.6 (3)	7.6 (3)	7.6 (3)	7.6 (3)	7.6 (3)	7.6 (3)
Powder Injection Port Filler/YSZ	Ext/ Int	Ext/ Int	Ext/ Int	Ext/ Int	Ext/ Int	Ext/ Int

Basic Equipment - Plasmadyne

- 0 Power Supply
 - Model #PS-61M
 - Open Circuit Voltage 80V
- 0 Gun
 - Model SG-1-B
 - Anode S1-3-F
 - Cathode S1-3-R
- 0 Powder Feeders
 - Rotofeed Model 1000A
 - Gears B

Table I Plasma Spray Parameters

<u>Coating System</u>	<u>Surface Roughness μ-in. (RMS) (After Machining)</u>
I-P	350-400
II-P	300-400
III-P	270-350
I-C	300-400
II-C	350-400
III-C	170-220

Additional Measurements: Sample I-P (Before Burnout or Machining)

<u>Condition</u>	<u>μ-in. (RMS)</u>
As Sprayed	300-350
Ground	80-120
Machined	160-200

Table II Surface Roughness Measurements

<u>Coating System</u>	<u>Hardness</u> <u>(Heat-Treated Condition)</u>	
	<u>Hardness Scale</u>	
	<u>R15W</u>	<u>R15Y</u>
I-P	6	13
II-P	81	89
III-P	43	61
I-C	63	78
II-C	72	82
III-C	81	85

Additional Hardness Determination - I-P
(Non-Heat Treated)

<u>Condition</u>	<u>R15Y</u>
As Sprayed	73
Machined	83
Ground	88

Table III Coating System Hardness

Coating System Designation	v/o ZrO ₂ %		Filler			
	Target	(Measured)	v/o Polyester %		v/o Cenospheres %	
	Target	(Measured)	Target	(Measured)	Target	(Measured)
I-P	65	(72)	35	(28)	0	---
II-P	75	(79)	25	(21)	0	---
III-P	80	(83)	20	(17)	0	---
I-C	50	(70)	0	---	50	(30)
II-C	40	(65)	0	---	60	(35)
III-C	30	(68)	0	---	70	(32)

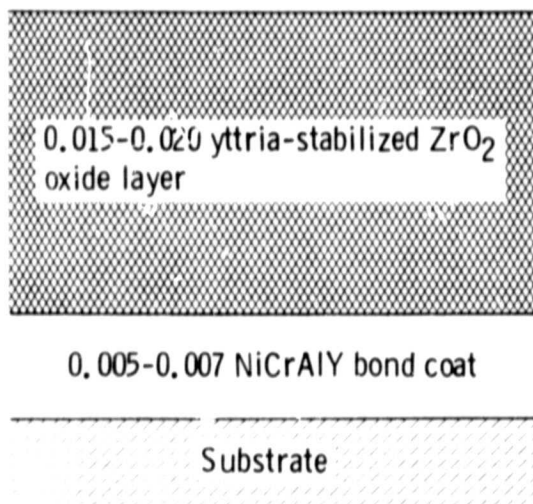
Table IV

Coating System Composition

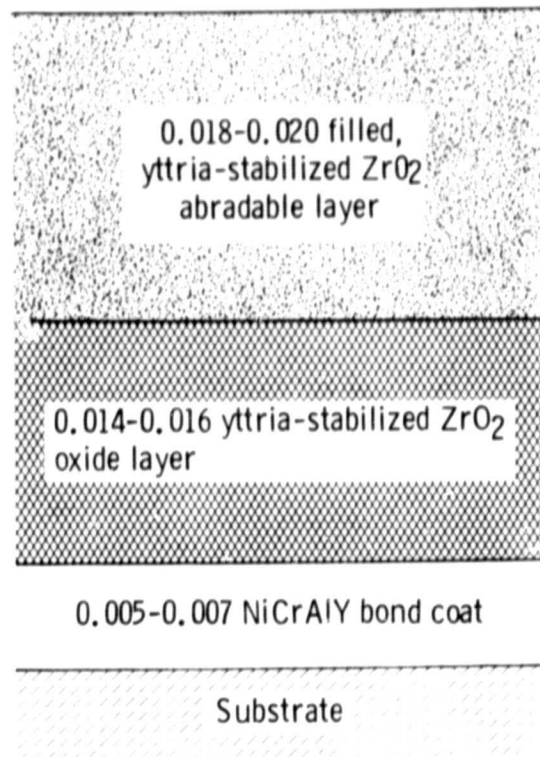
<u>Seal System</u>	<u>Rub Depth cm (Inch)</u>	<u>Change in Blade Length cm (Inch)</u>	<u>Normal Force Newtons (lbs.)</u>	<u>Tangential Force Newtons (lbs.)</u>
I-P-S	0.013 (0.005)	0	---	5.12 (1.15)
I-P-F	0.053 (0.021)	-0.005 (-0.002)	---	20.82/47.95 (4.68)/(10.78)
II-P-S	0.038 (0.015)	-0.0005 (-0.0002)	11.61 (2.61)	6.98 (1.57)
II-P-F	0.013 (0.005)	-0.0015 (-0.0006)	52.22 (11.74)	28.24 (6.35)
III-P-S	0.038 (0.015)	0	25.93 (5.83)	11.30 (2.54)
III-P-F	0.041 (0.016)	-0.003 (-0.001)	35.58 (8.0)	28.60 (6.43)
I-C-S	0.013 (0.005)	-0.003 (-0.001)	11.25 (2.53)	7.34 (1.65)
I-C-F	---	---	---	---
II-C-S	0.030 (0.012)	-0.0005 (-0.0002)	28.2 (6.3)	31.14 (7.0)
II-C-F	---	---	---	---
III-C-S	0.023 (0.009)	-0.0015 (-0.0006)	20.15 (4.53)	29.80 (6.7)
III-C-F	---	---	---	---

Table V Summary of Abradability Tests

REPRODUCIBILITY OF THE
ORIGINAL PAGE IS POOR



(a) Typical NASA duplex
thermal barrier coating



(b) Dual-density/composition abrasion-resistant
thermal barrier coating

Figure 1 Cross sections of thermal barrier coating configurations

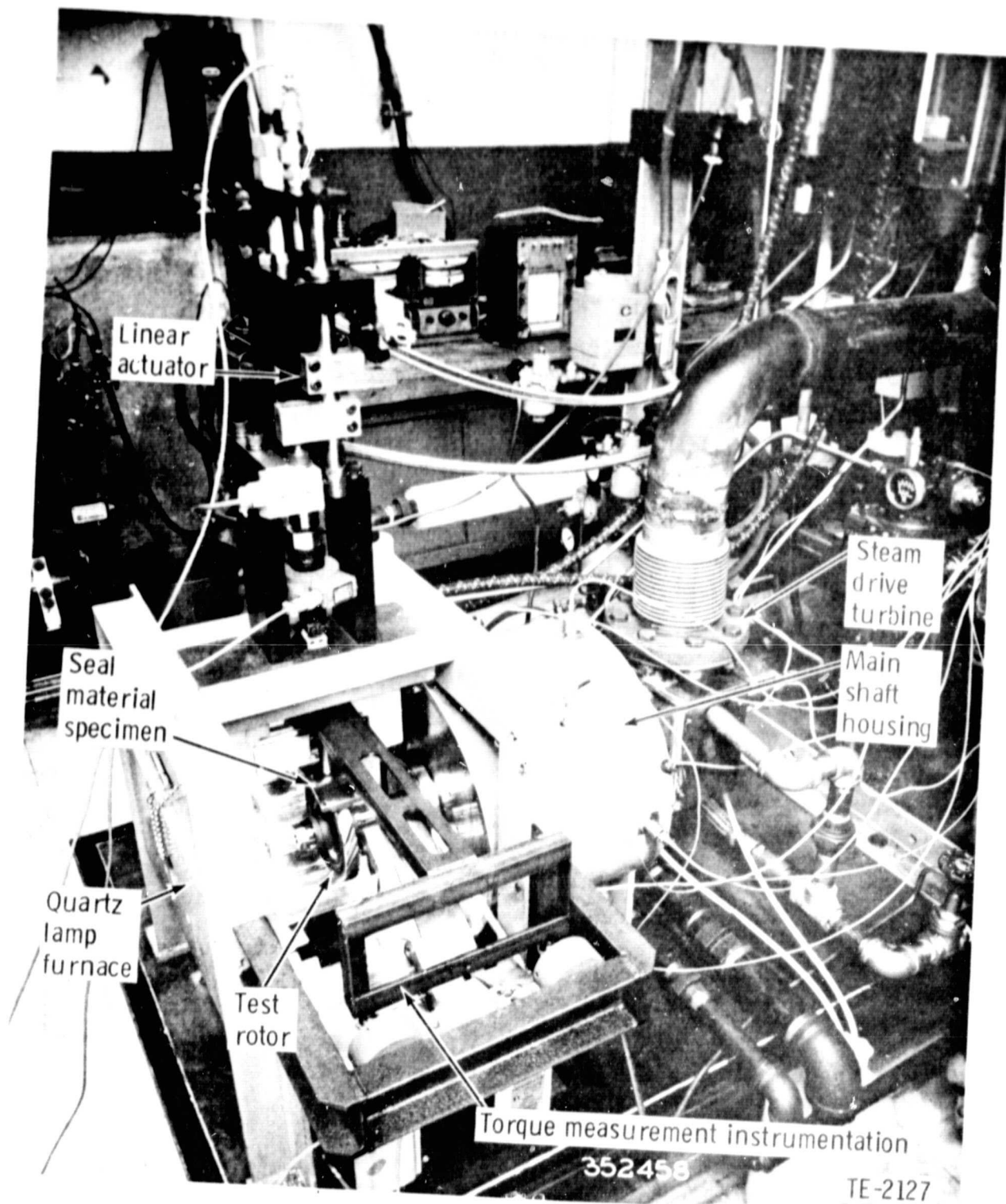


Figure 2 High-speed/high-temperature abrasable seal materials test rig

REPRODUCIBILITY OF THE
ORIGINAL PAGE IS POOR

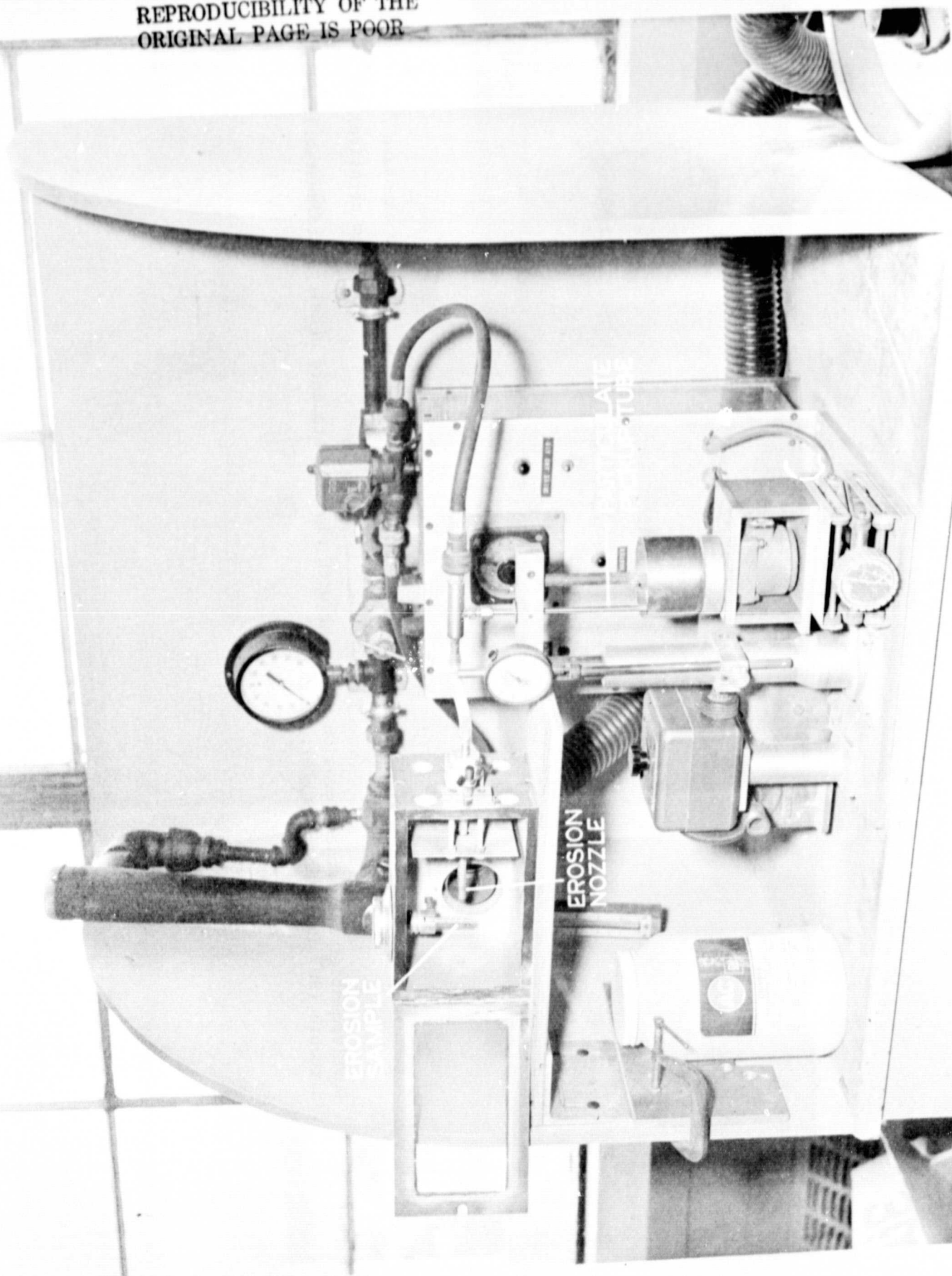


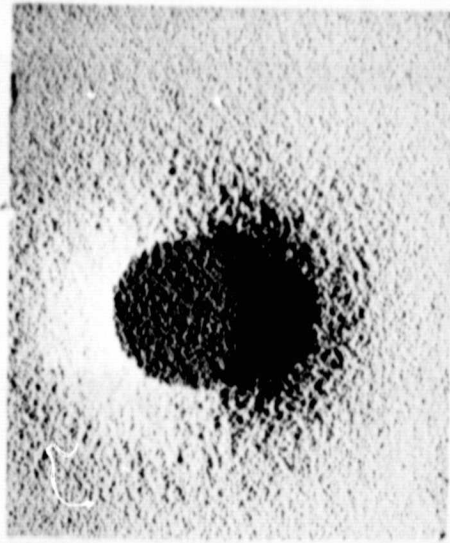
Figure 3 Erosion Test Rig



a. As machined



b. 30 min. exposure
(12.1 gm abrasive)

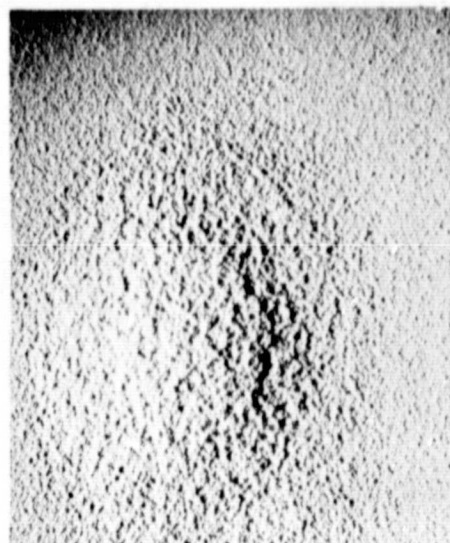


c. 60 min. exposure
(23.1 gm abrasive)

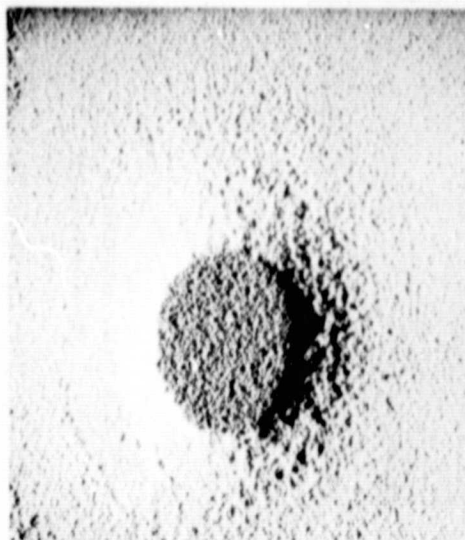
Figure 4 Development of accelerated erosion wear scar with time for standard density yttria-stabilized zirconia (90° impingement angle). Magn: 3X



a. 30 min. exposure
(5.4 gm abrasive)



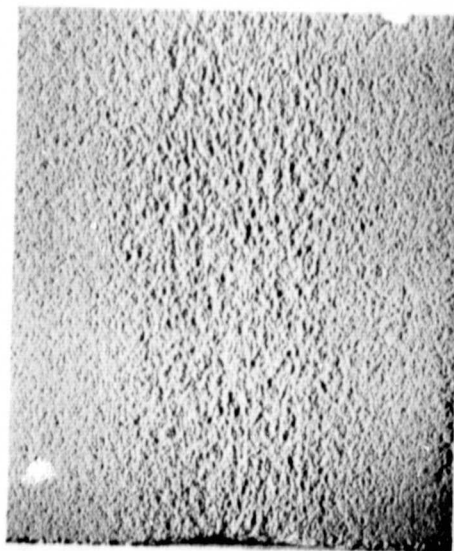
b. 60 min. exposure
(14.7 gm abrasive)



c. 120 min. exposure
(38.1 gm abrasive)

Figure 5 Development of accelerated erosion wear scar with time for standard density yttria-stabilized zirconia (45° impingement angle) Magn: 3X

REPRODUCIBILITY OF THE
ORIGINAL PAGE IS POOR



a. 30 min. exposure
(10.1 gm abrasive)



b. 60 min. exposure
(21.3 gm abrasive)



c. 120 min. exposure
(43.5 gm abrasive)

Figure 6 Development of accelerated erosion wear scar with time for standard density yttria-stabilized zirconia
(15° impingement angle) Magn: 3X

REPRODUCIBILITY OF THE
ORIGINAL PAGE IS POOR

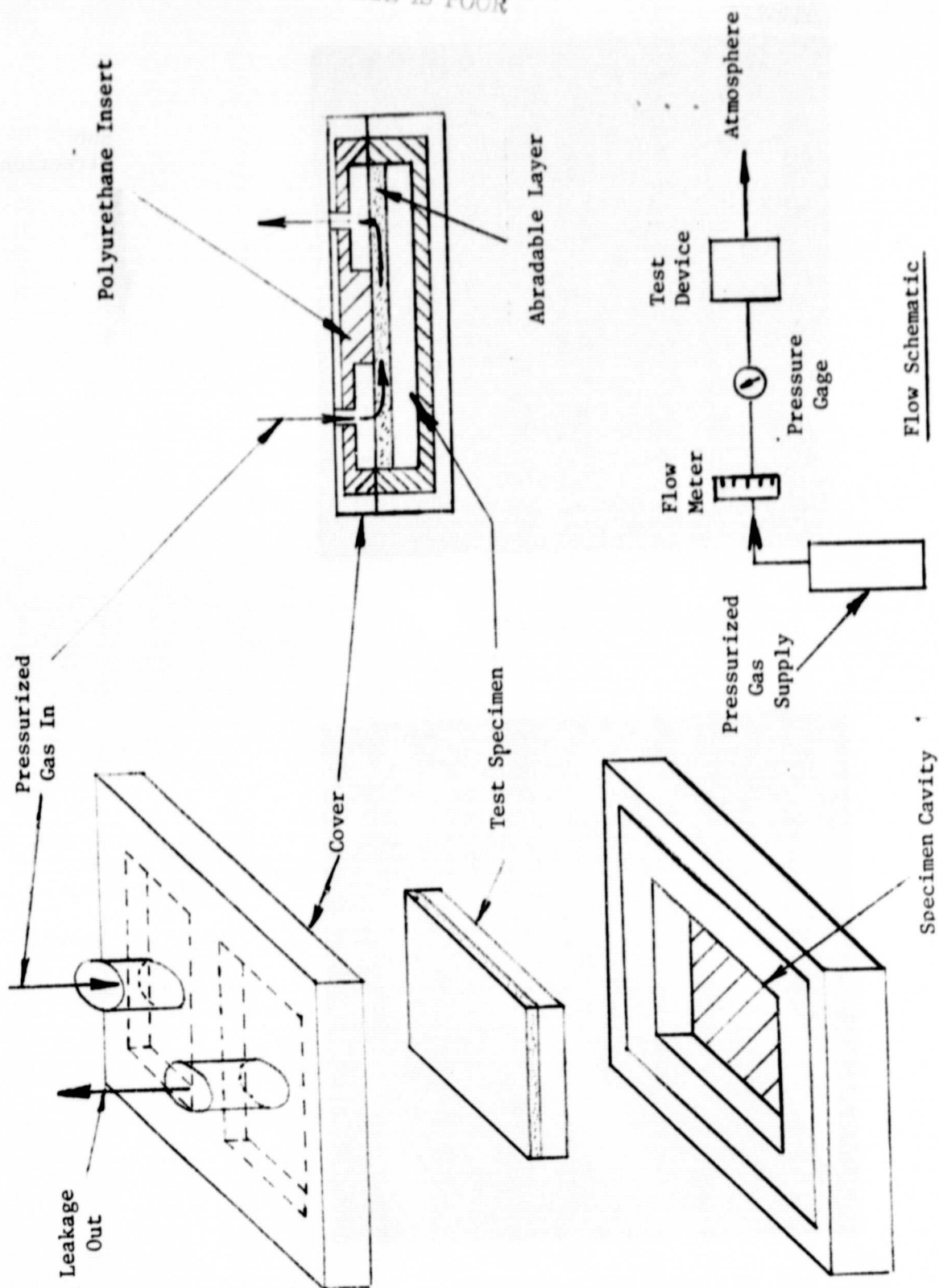
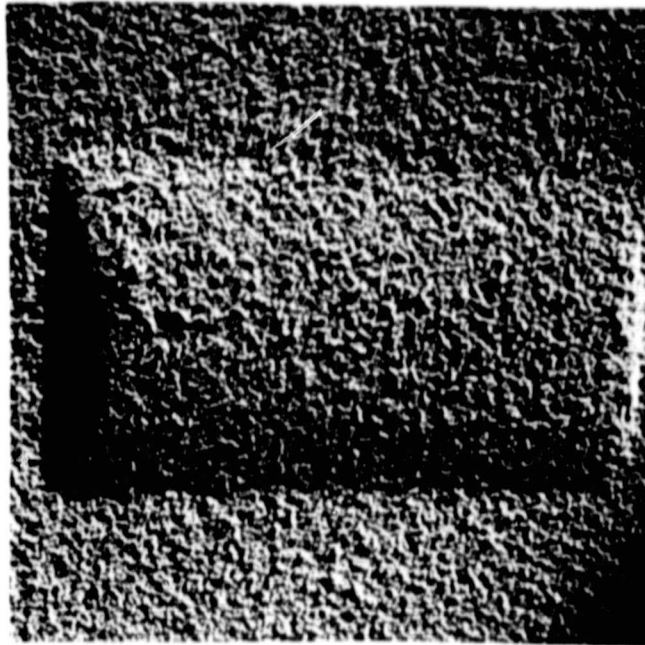


Figure 7 Permeability Test Device



Rub
Direction



Blade track wear scar



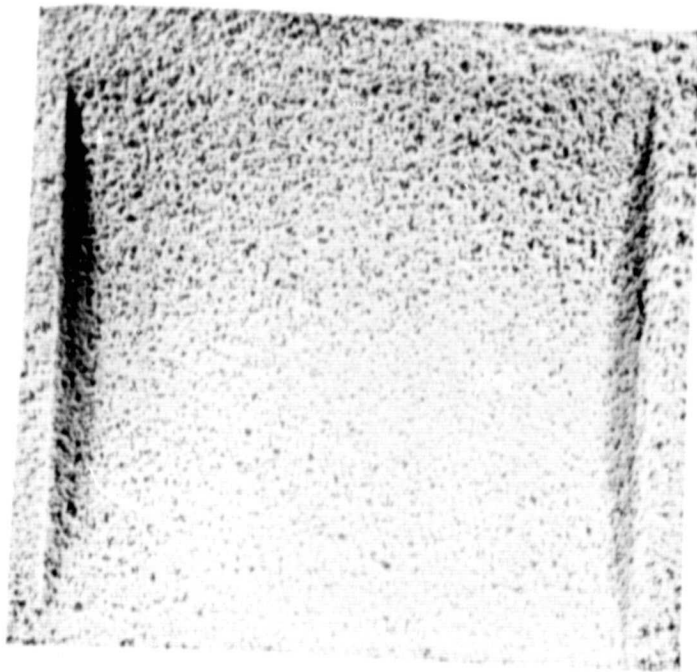
Incursion rate:
.0025 cm/sec
(.001 in/sec)

Blade tip speed:
229 m/sec
(750 ft/sec)

Blade tip condition

Figure 8 Slow incursion rate abrasability test results for specimen configuration I-P Magn: 5X

REPRODUCIBILITY OF THE
ORIGINAL PAGE IS POOR



Blade track wear scar



Rub
Direction

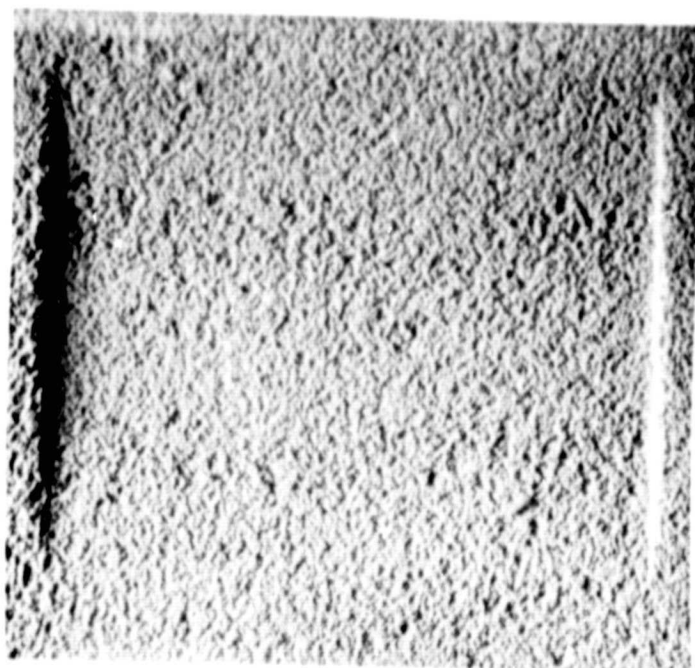


Incursion rate:
.0025 cm/sec
(.001 in/sec)

Blade tip speed:
229 m/sec
(750 ft/sec)

Blade tip condition

Figure 9 Slow incursion rate abrasability test results
for specimen configuration II-P Magn: 5X



Rub
Direction

Blade track wear scar

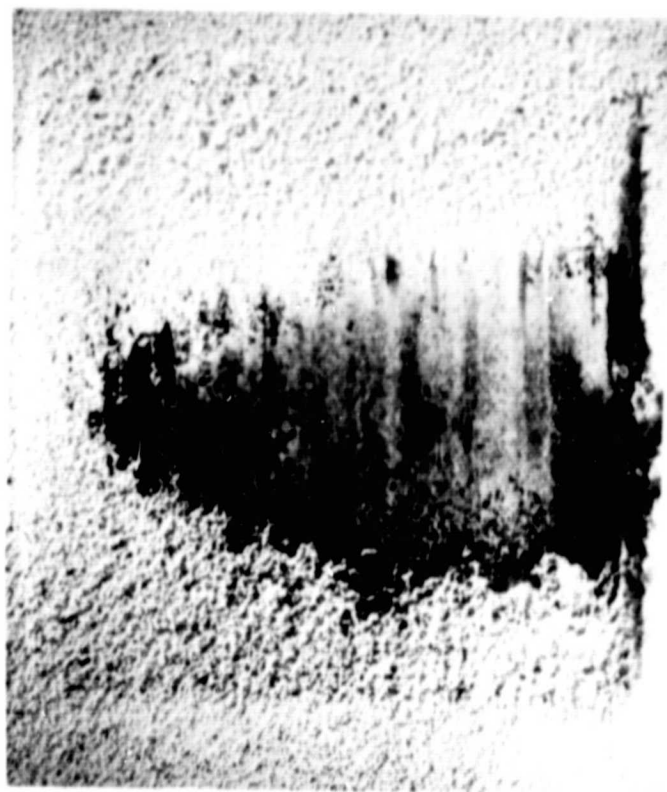


Incursion rate:
.0025 cm/sec
(.001 in/sec)

Blade tip speed:
229 m/sec
(750 ft/sec)

Blade tip condition

Figure 10 Slow incursion rate abrasability test results for specimen configuration III-P Magn: 5X

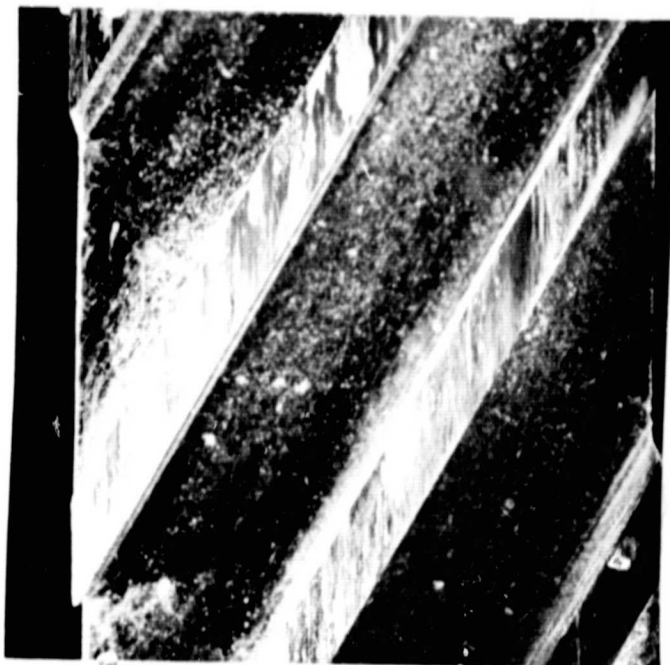


Blade track wear scar



Rub
Direction

REPRODUCTION OF THE
ORIGINAL PAGE IS POOR

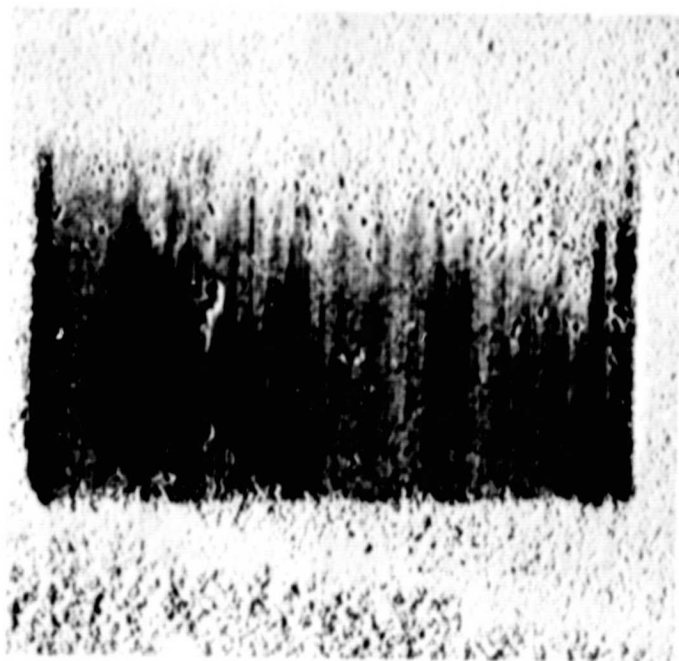


Blade tip condition

Incursion rate:
.025 cm/sec
(.010 in/sec)

Blade tip speed:
229 m/sec
(750 ft/sec)

Figure 11 Fast incursion rate abrasability test results for specimen configuration I-P Magn: 5X



Rub
Direction

Blade track wear scar

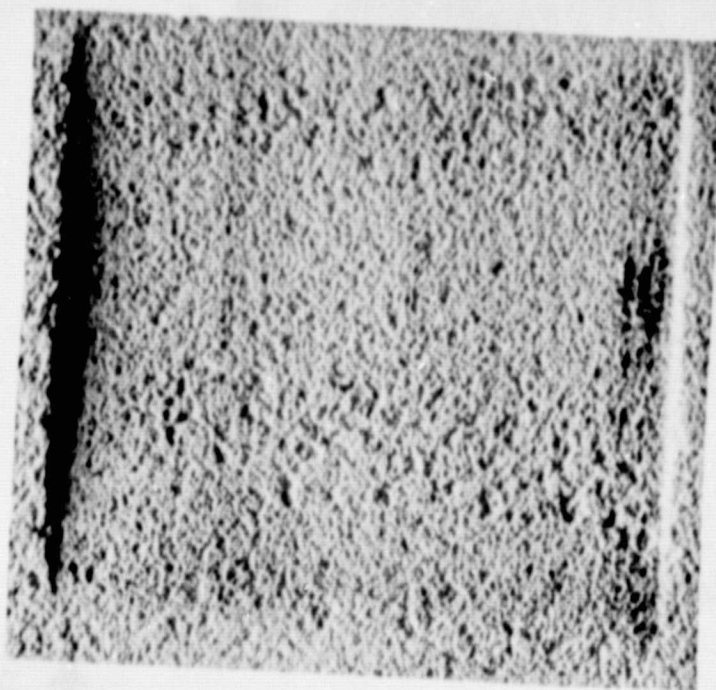


Incursion rate:
.025 cm/sec
(.010 in/sec)

Blade tip speed:
229 m/sec
(750 ft/sec)

Blade tip condition

Figure 12 Fast incursion rate abrasability test results for specimen configuration II-P Magn: 5X

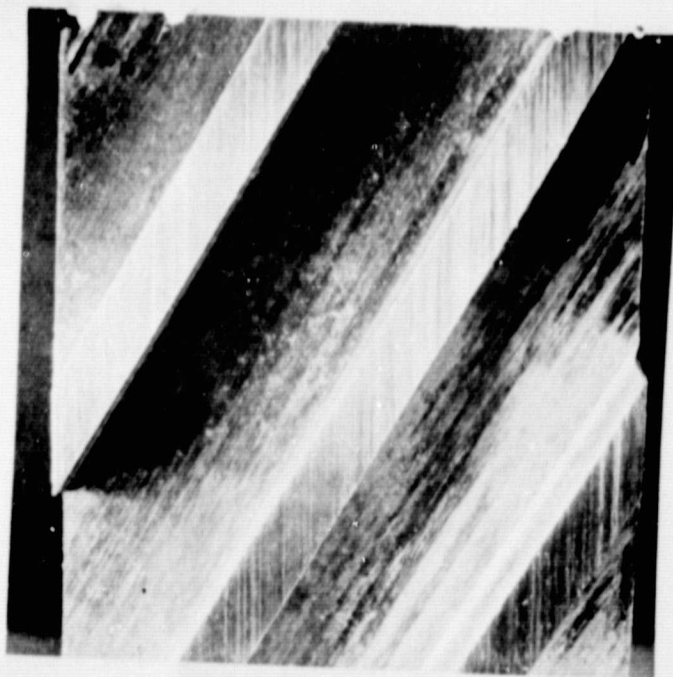


Blade track wear scar



Rub
Direction

REPRODUCIBILITY OF THE
ORIGINAL PAGE IS POOR

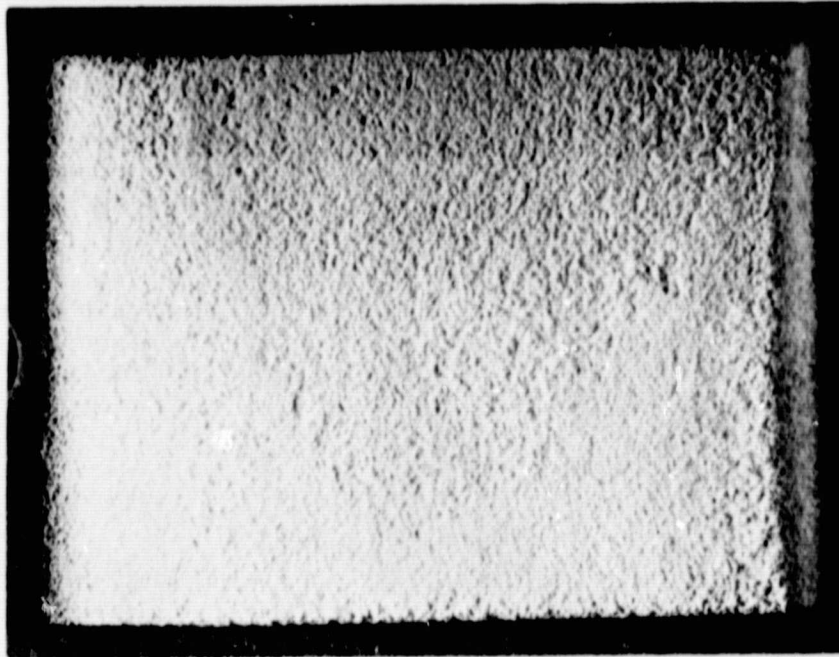


Blade tip condition

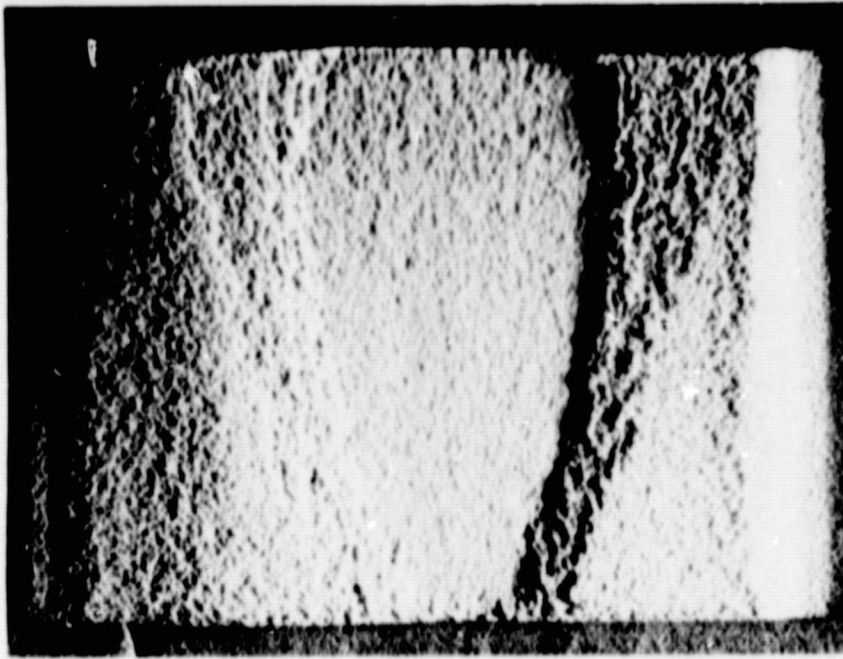
Incursion rate:
.025 cm/sec
(.010 in/sec)

Blade tip speed:
229 m/sec
(750 ft/sec)

Figure 13 Fast incursion rate abrasability test results for
specimen configuration III-P Magn: 5X



a. As machined plus thermal decomposition of filler

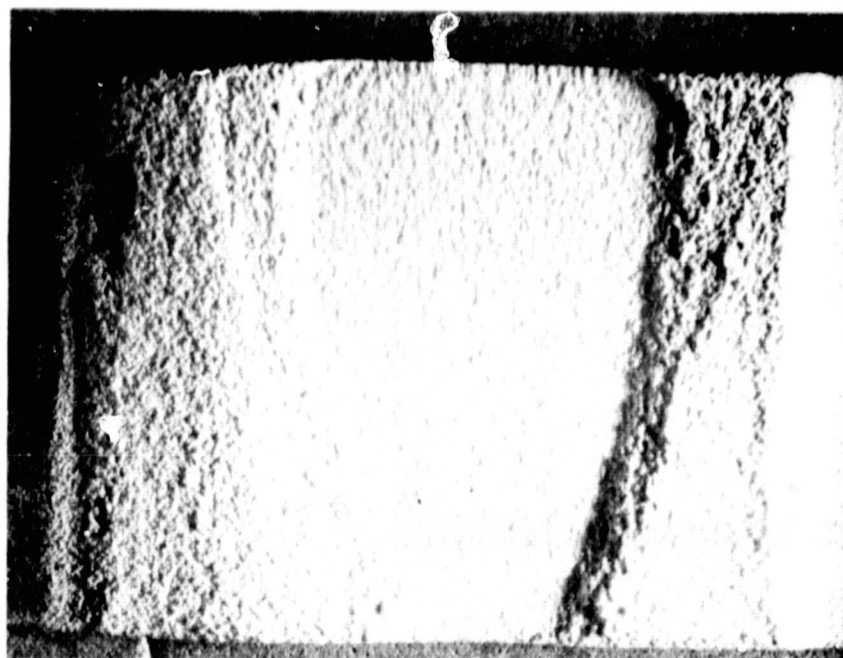


b. 30 min. exposure (12.5 gm abrasive)



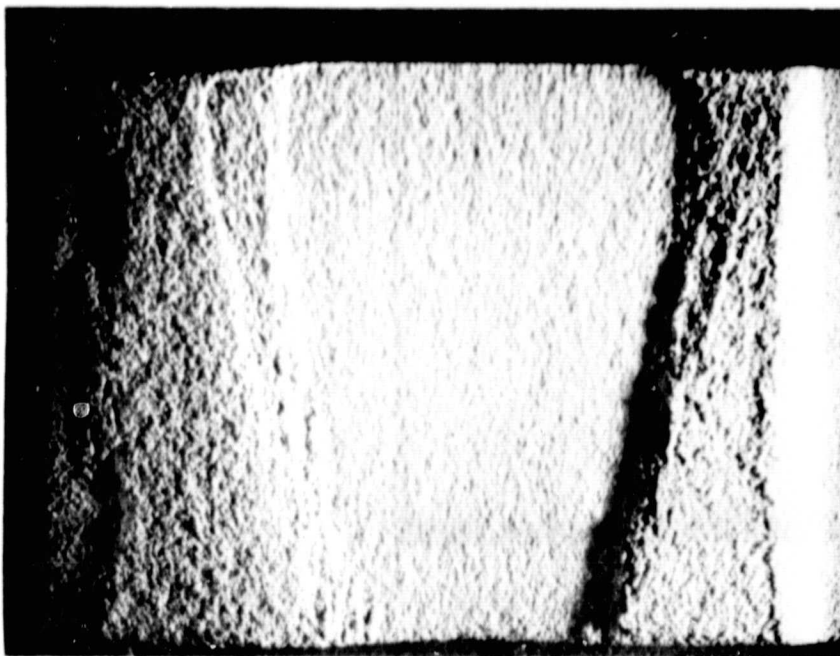
Flow direction

Figure 14 Development of accelerated erosion wear scar with time for coating system I-P Magn: 3X



c. 60 min. exposure (27.5 gm abrasive)

REPRODUCIBILITY OF THE
ORIGINAL F...

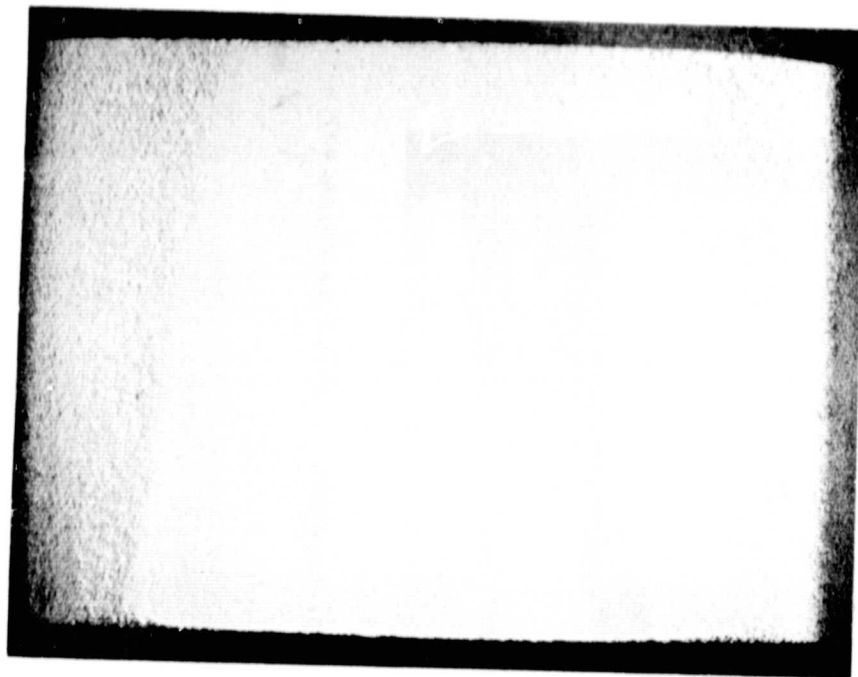


d. 120 min. exposure (41.7 gm abrasive)

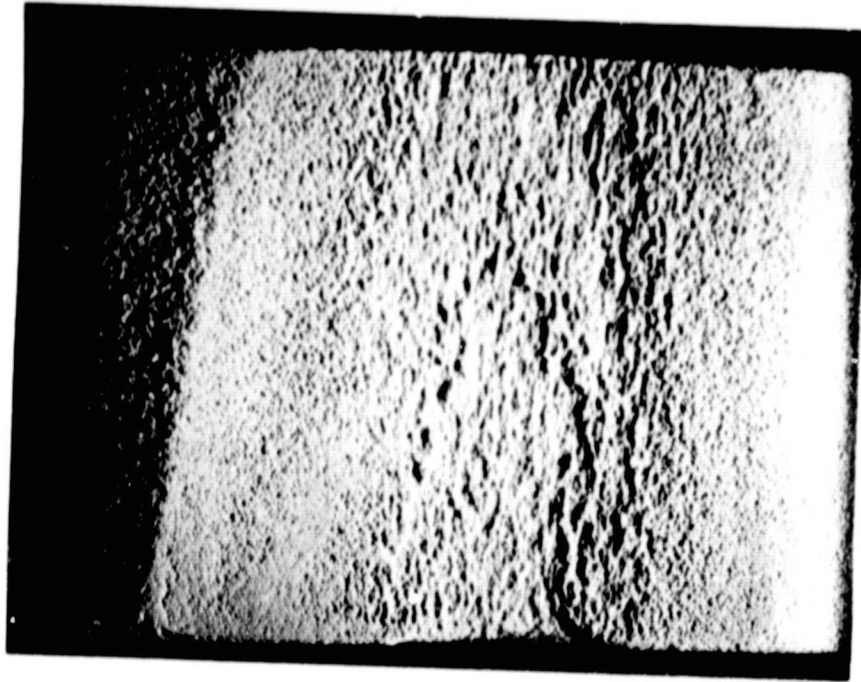


Flow direction

Figure 14 (cont'd) Development of accelerated erosion wear scar with time for coating system
I-P Magn: 3X



a. As machined plus thermal decomposition of filler



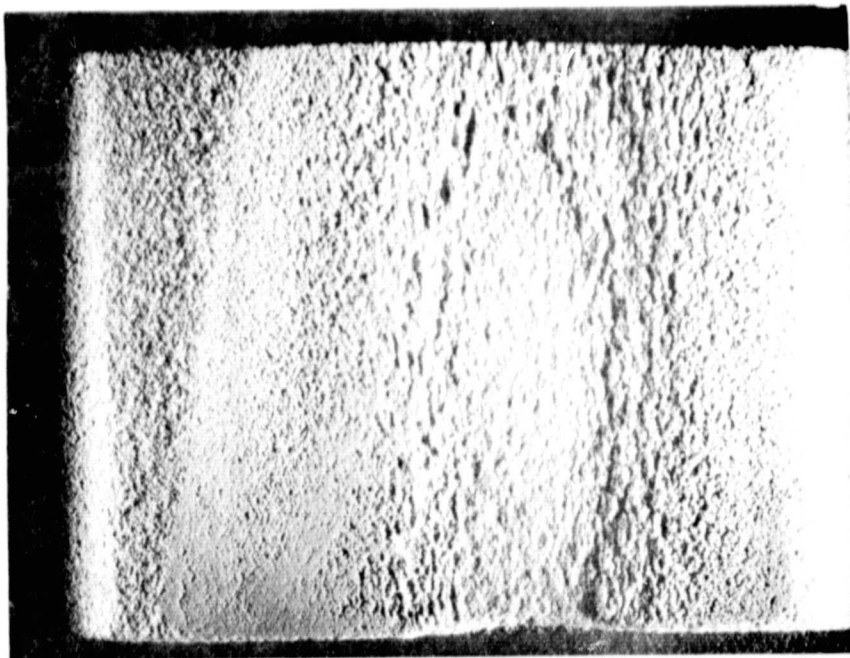
b. 20 min. exposure (13.4 gm abrasive)



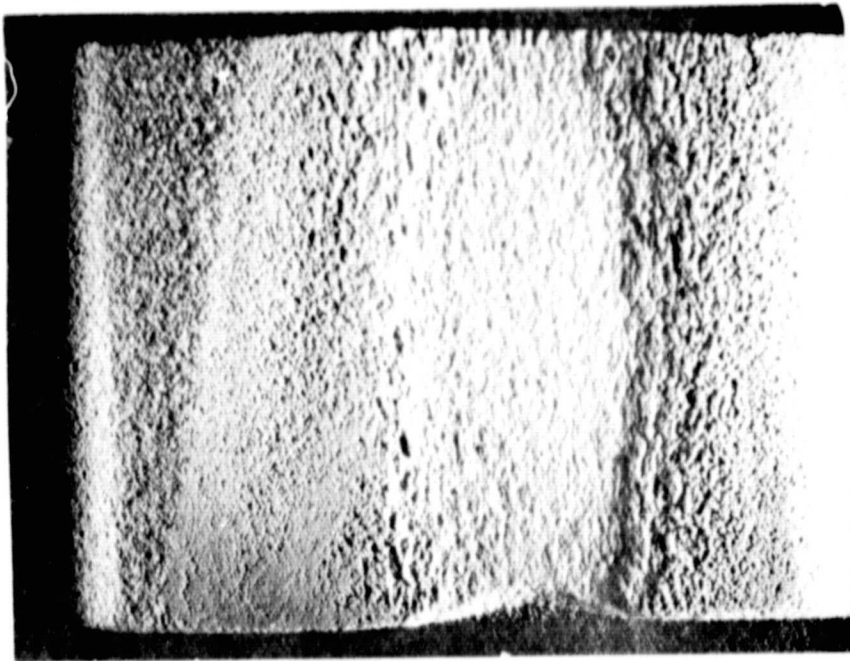
Flow direction

Figure 15 Development of accelerated erosion wear scar with time for coating system II-P Magn: 3X

REPRODUCIBILITY OF THE
ORIGINAL PAGE IS POOR



c. 60 min. exposure (19.1 gm abrasive)



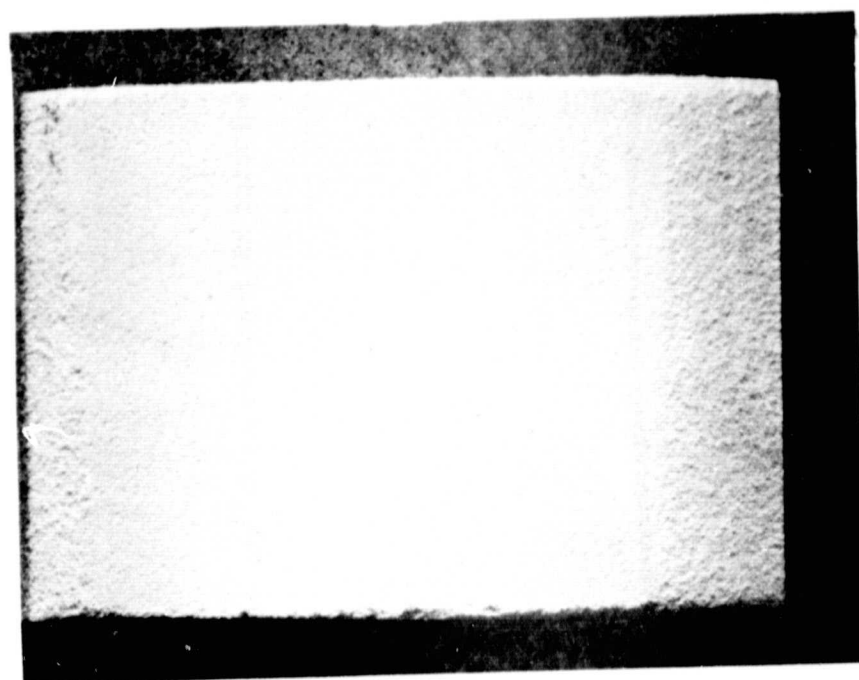
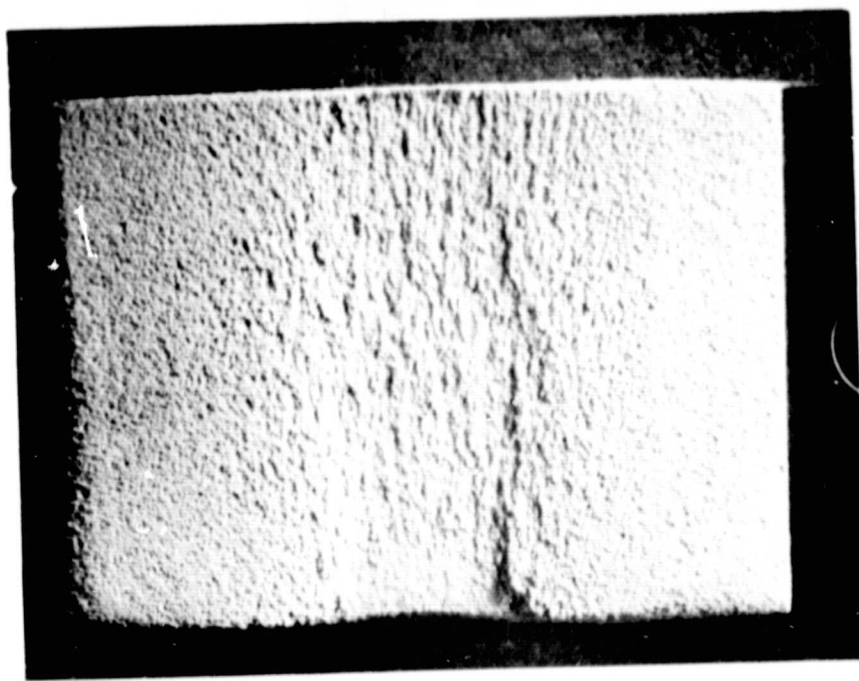
d. 120 min. exposure (37.8 gm abrasive)



Flow direction

Figure 15 cont'd

Development of accelerated erosion wear scar with time for coating system II-P
Magn: 3X

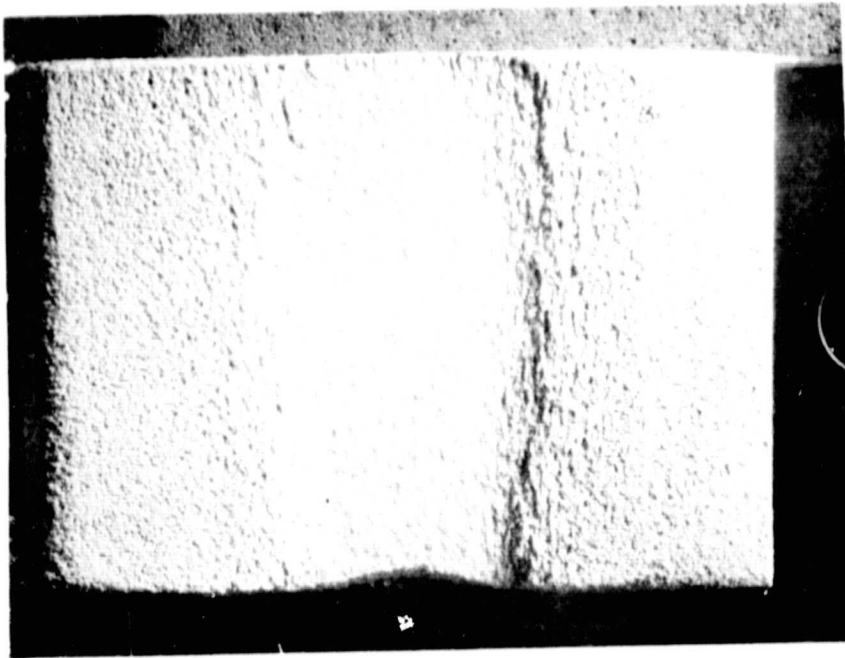


a. As machined plus thermal decomposition of filler

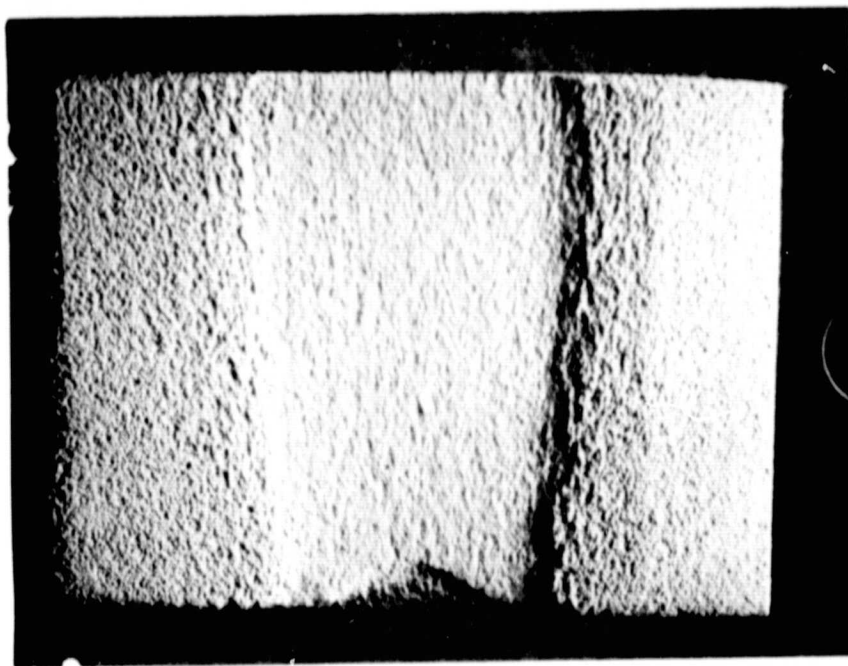
b. 30 min. exposure (7.4 gm abrasive)

Flow direction
↑

Figure 16 Development of accelerated erosion wear scar with time for coating system III-P Magn: 3X



c. 60 min. exposure (18.4 gm abrasive)



d. 120 min. exposure (45.8 gm abrasive)

Figure 16 Development of accelerated erosion wear scar with time for coating system III-P Magn: 3X
cont'd

REPRODUCIBILITY OF THE
ORIGINAL SCAR

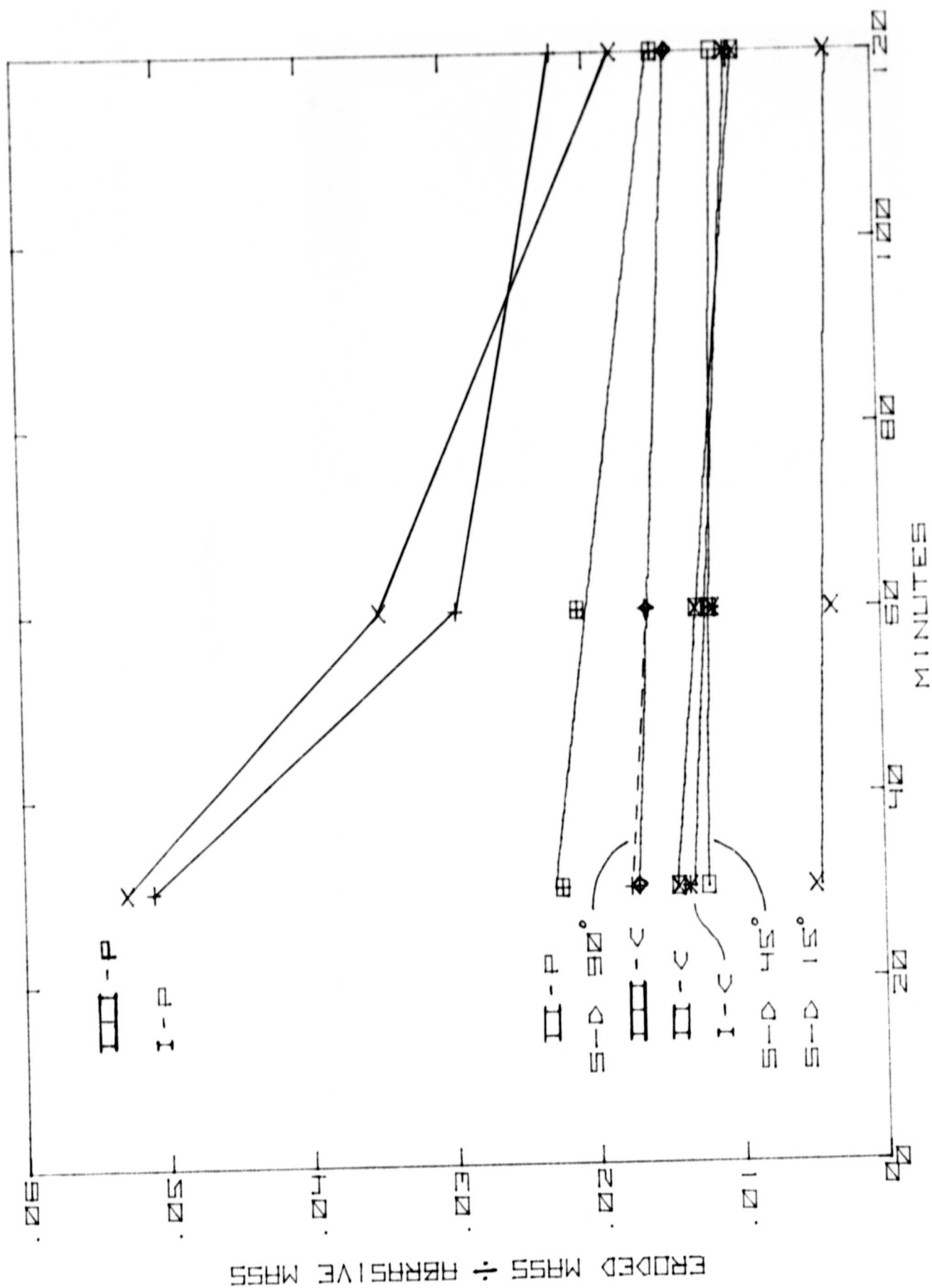


Figure 17 Erosion of Polyester and Cenosphere filled YSZ systems

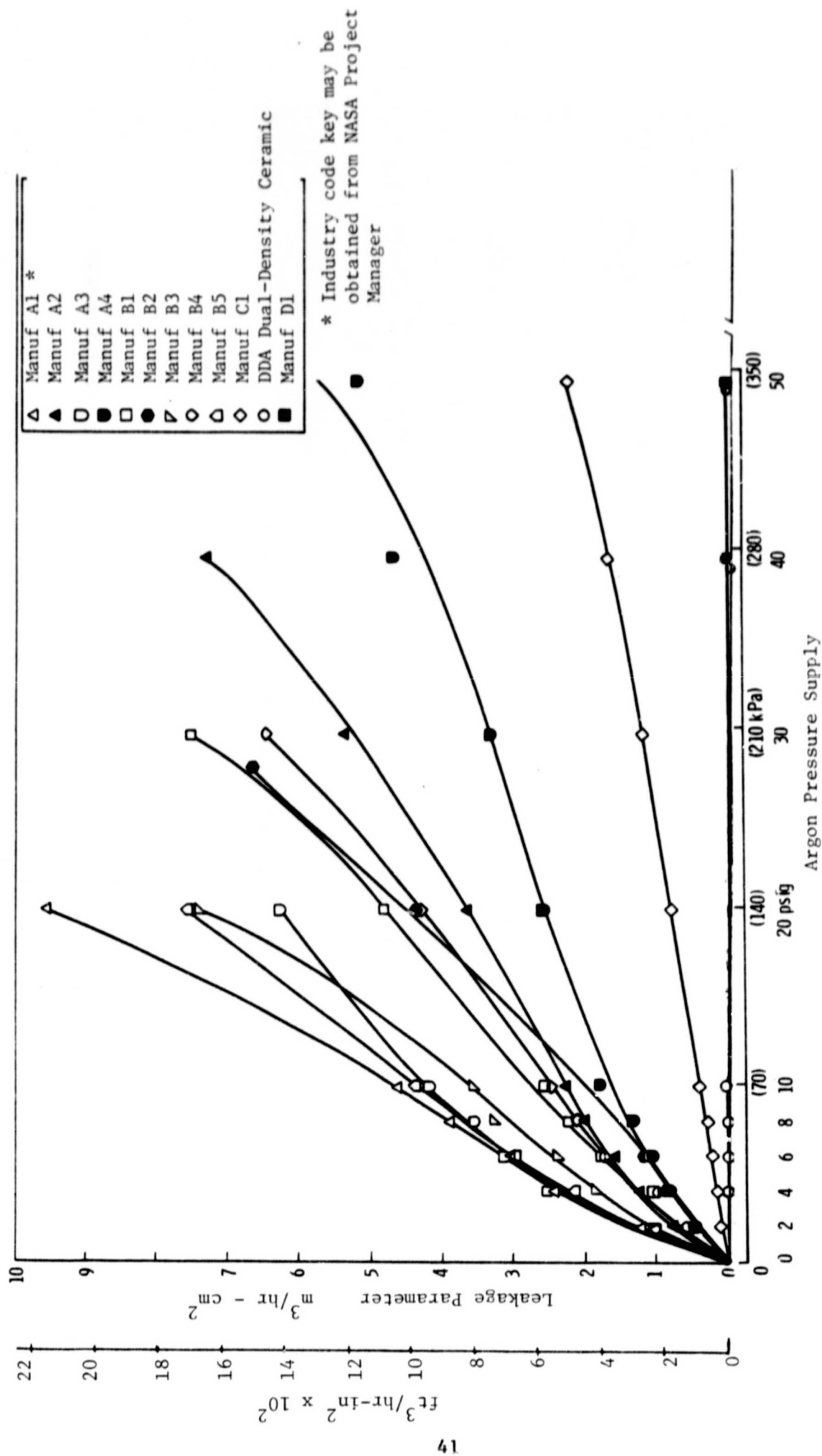
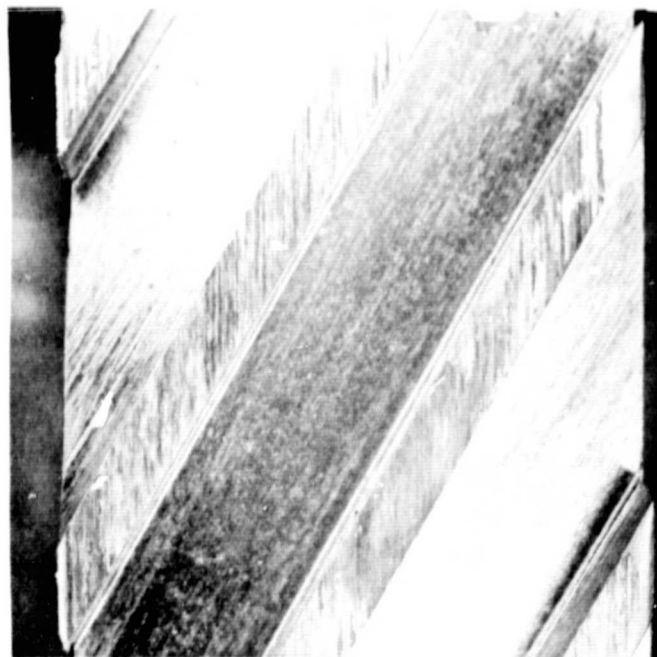


Figure 18 Abradable Seal Material Permeability



Blade track wear scar

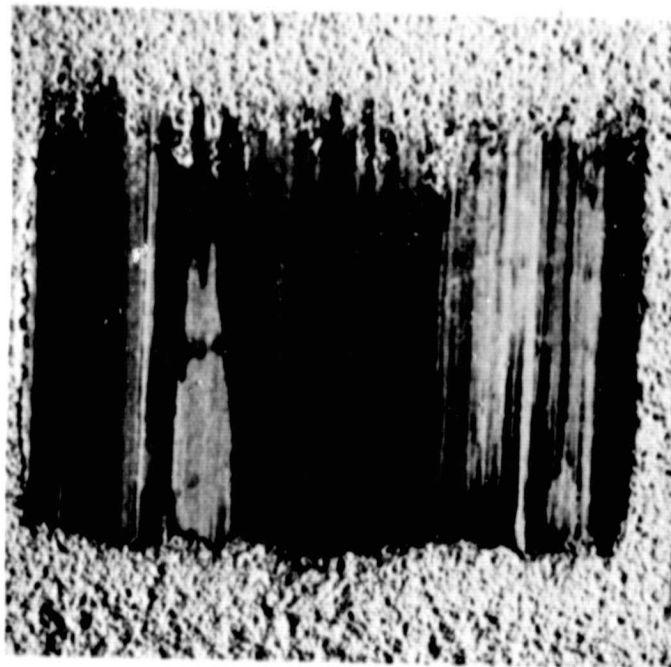


Incursion rate:
.0025 cm/sec
(.001 in/sec)

Blade Tip speed:
229 m/sec
(750 ft/sec)

Blade tip condition

Figure 19 Slow incursion rate abrasability test results for specimen configuration I-C Magn: 5X



Rub
Direction

Blade track wear scar



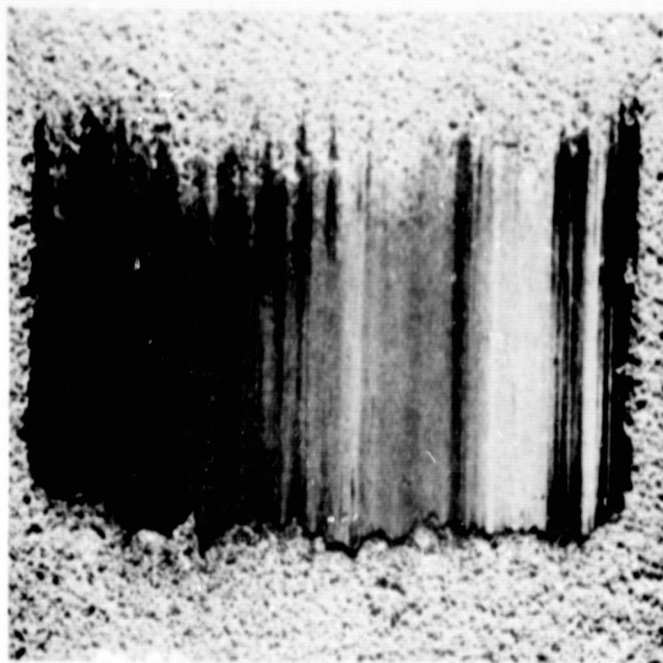
Incursion rate:
.0025 cm/sec
(.001 in/sec)

Blade tip speed:
229 m/sec
(750 ft/sec)

Blade tip condition

Figure 20 Slow incursion rate abrasability test results for specimen configuration II-C Magn: 5X

REPRODUCIBILITY OF THE
ORIGINAL PAGE IS POOR



Rub
Direction

Blade track wear scar



Incursion rate:
.0025 cm/sec
(.001 in/sec)

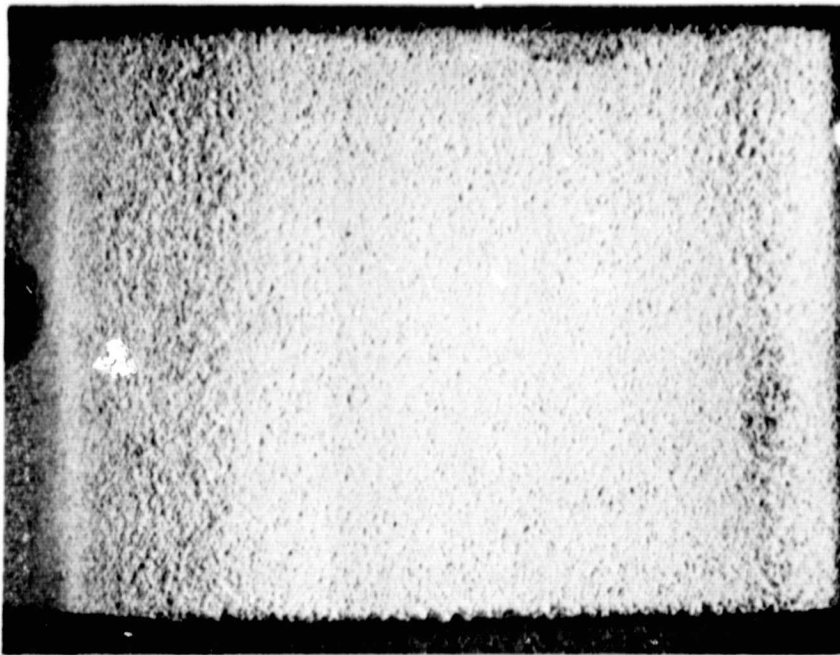
Blade tip speed:
229 m/sec
(750 ft/sec)

Blade tip condition

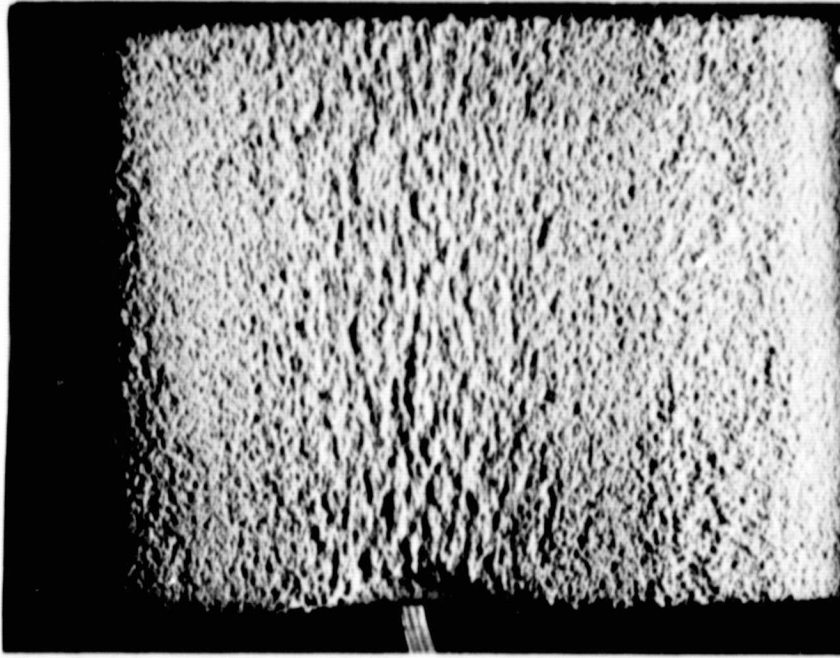
Figure 21

Slow incursion rate abrasability test results for specimen
configuration III-C Magn: 5X

REPRODUCIBILITY OF THE
ORIGINAL PAGE IS POOR



a. As machined

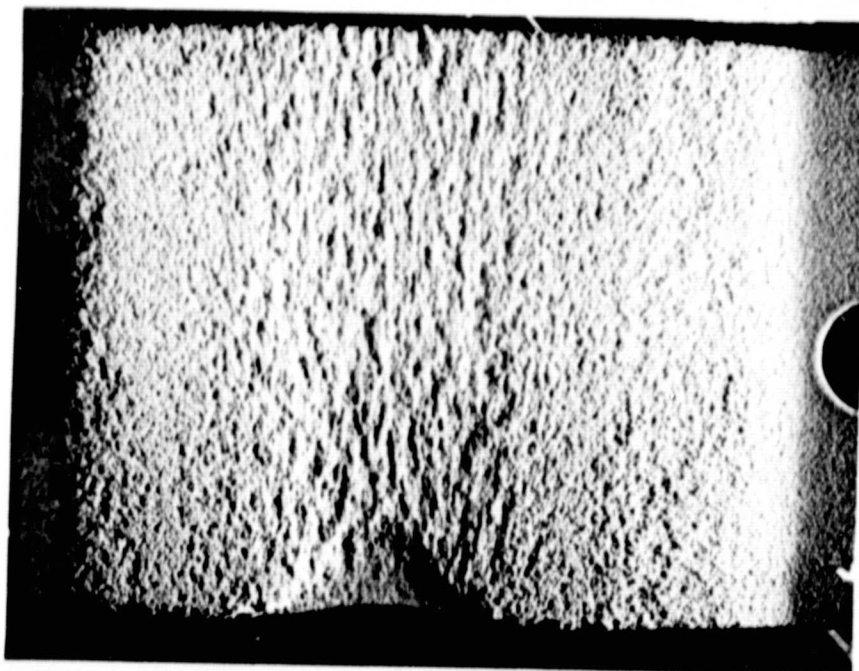


b. 30 min. exposure (9.3 gm abrasive)

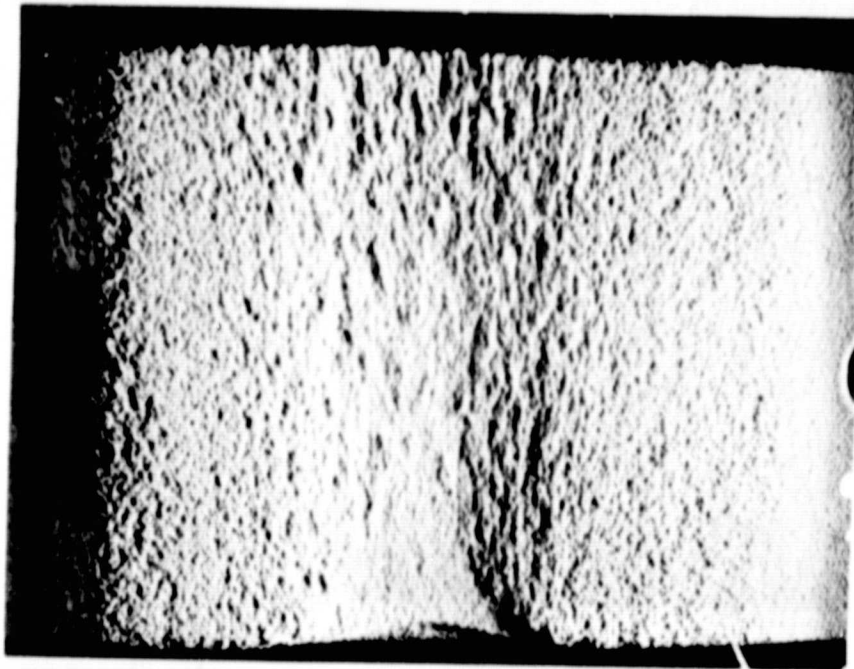


Flow direction

Figure 22 Development of accelerated erosion wear scar with time for coating system I-C Magn: 3X



c. 60 min. exposure (22.8 gm abrasive)



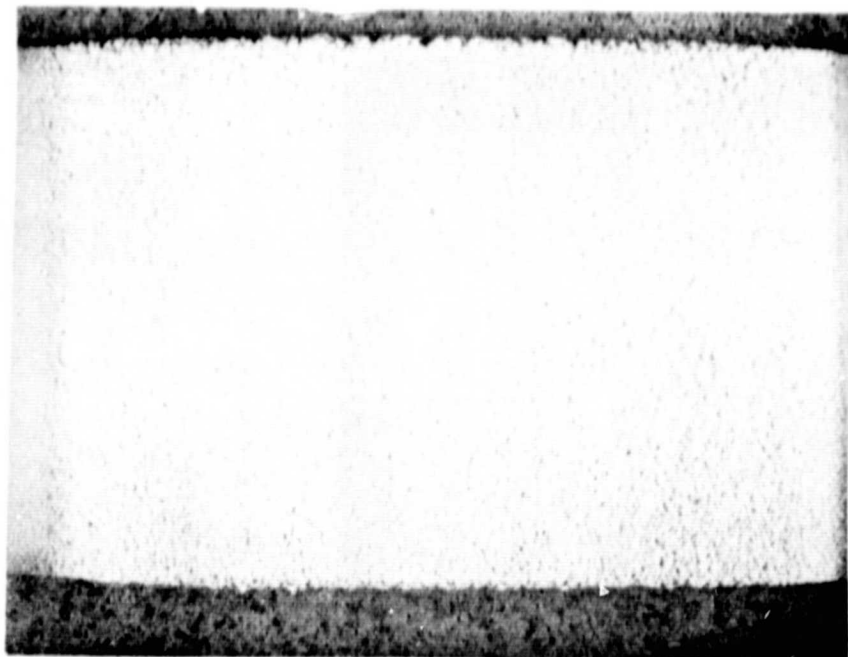
d. 120 min. exposure (50.3 gm abrasive)



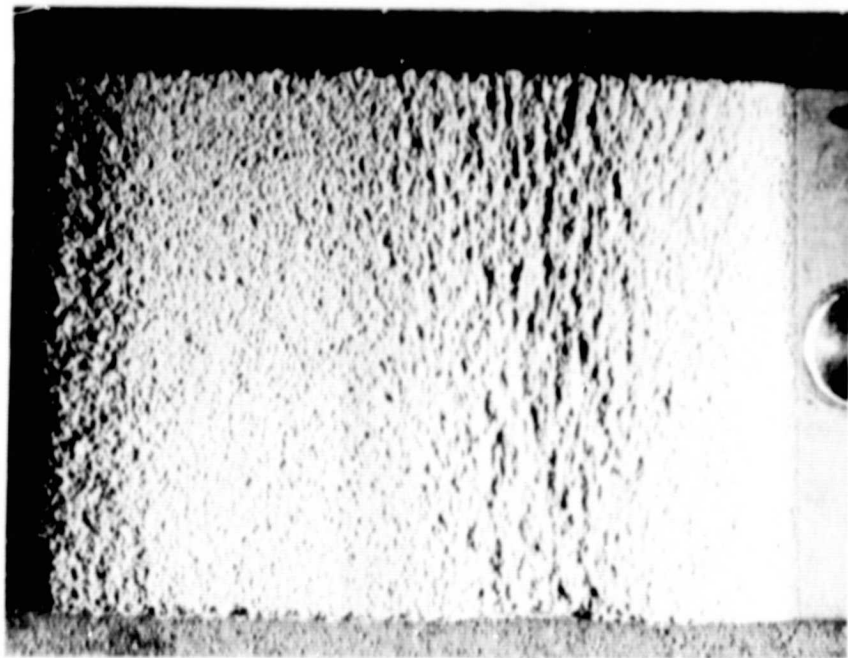
Flow direction

Figure 22 cont'd.

Development of accelerated erosion wear scar with time for coating system I-C
Magn: 3X



a. As machined

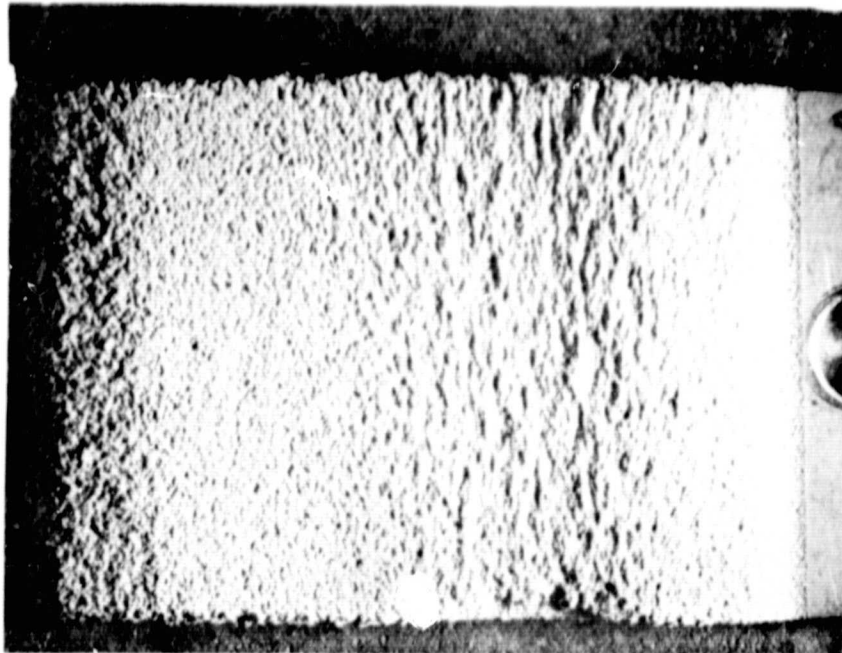


b. 30 min. exposure (7.1 gm abrasive)

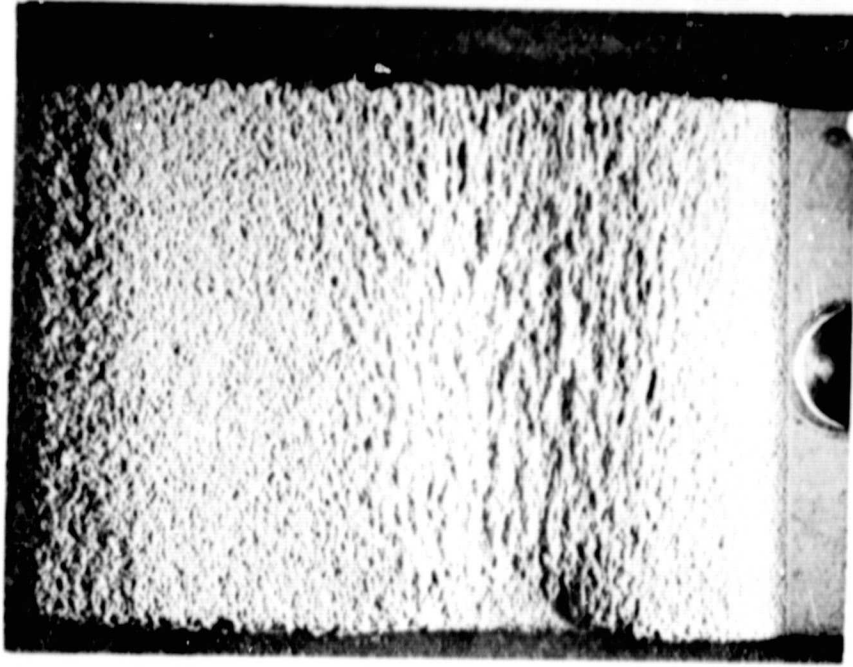


Figure 23 Development of accelerated erosion wear scar with time for coating system II-C Magn: 3X

REPRODUCIBILITY OF THE
ORIGINAL PAGE IS POOR



c. 60 min. exposure (17.0 gm abrasive)



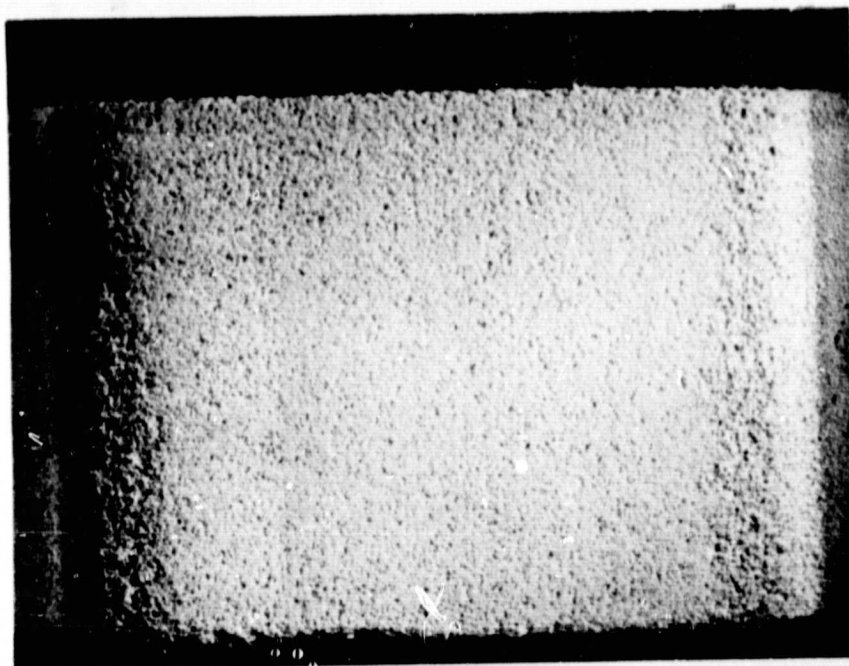
d. 120 min. exposure (42.2 gm abrasive)



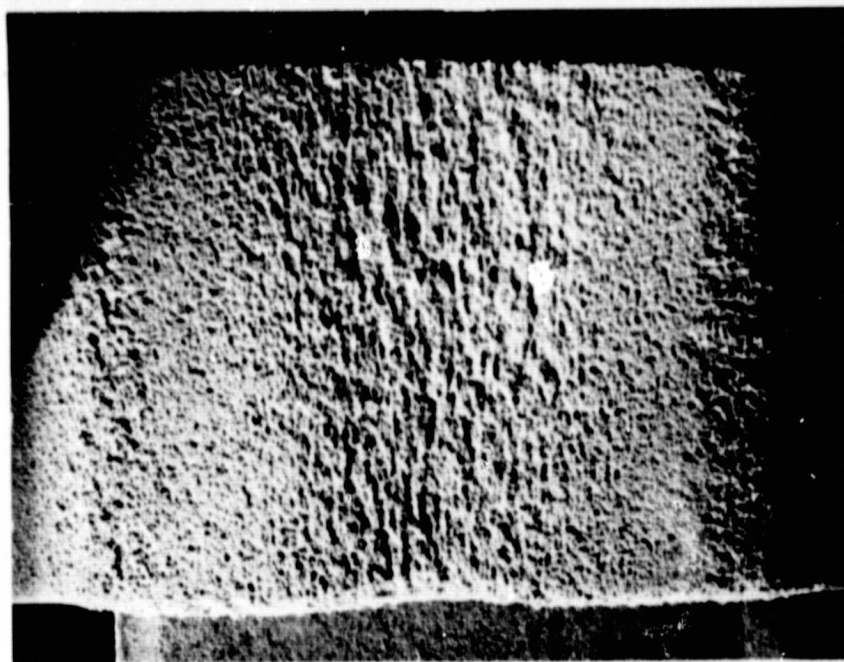
Flow direction

Figure 23 (cont.) Development of accelerated erosion wear scar with time for coating system II-C Magn: 3X

REPRODUCIBILITY OF THE
ORIGINAL PAGE IS POOR



a. As machined

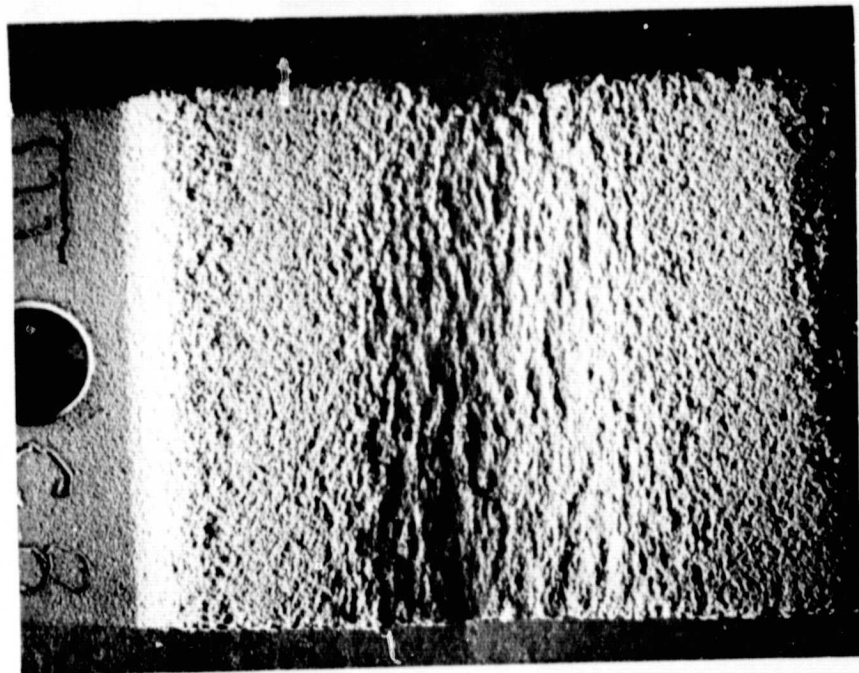


b. 30 min. exposure (16.4 gm abrasive)

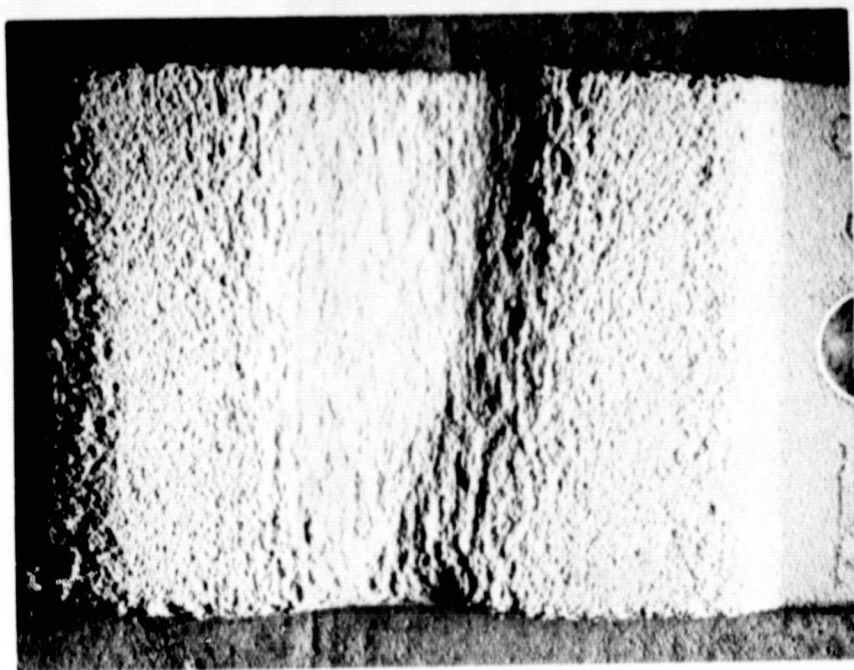


Flow direction

Figure 24 Development of accelerated erosion wear scar with time for coating system III-C Magn: 3X



c. 60 min. exposure (33.3 gm abrasive)



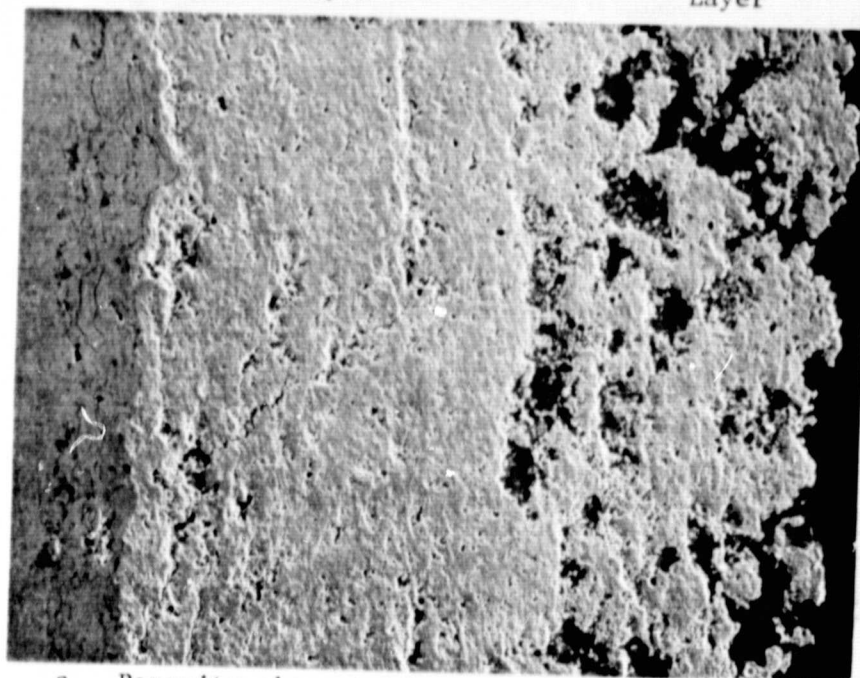
d. 120 min. exposure (63.1 gm abrasive)



Flow direction

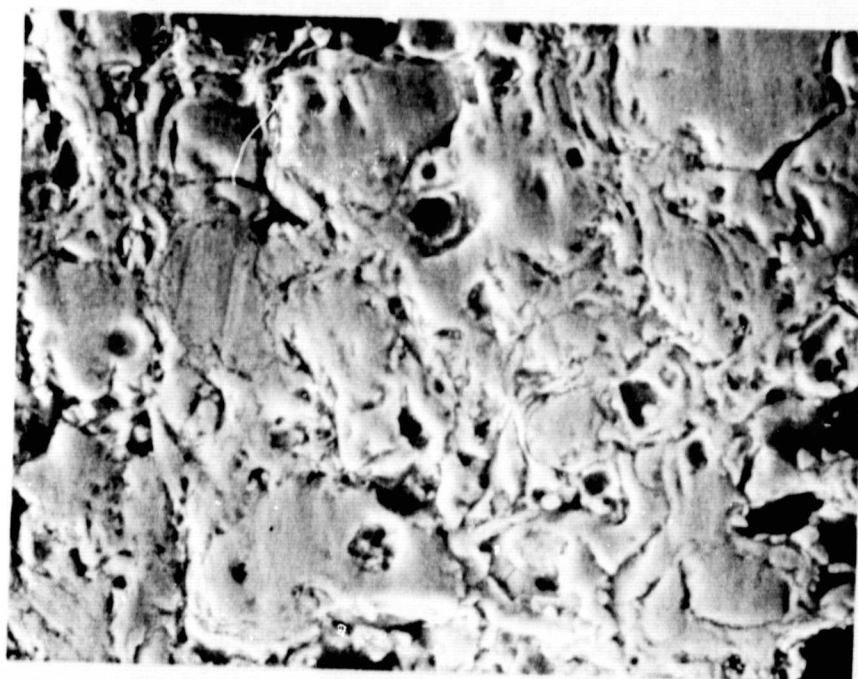
Figure 2/4 cont'd Development of accelerated erosion wear scar with time for coating system III-C Magn: 3X

Bond Coat	Standard Density Layer	Porous Oxide Layer
--------------	------------------------------	--------------------------



Magn:
100X

a. Porosity characteristics



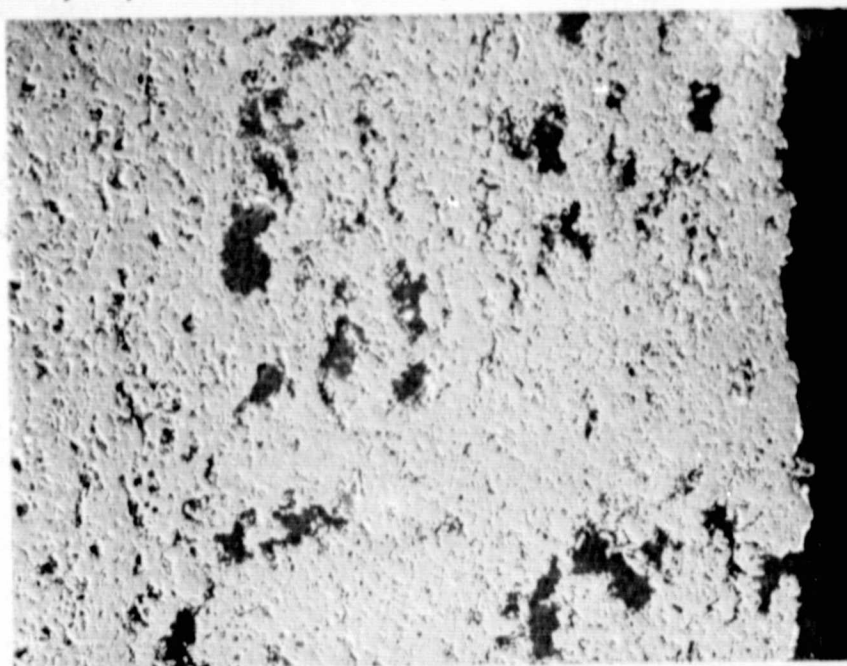
Magn:
1000X

b. Ceramic particle morphology (outer layer)

Figure 25 Porosity characteristics and ceramic particle morphology of coating system I-P.

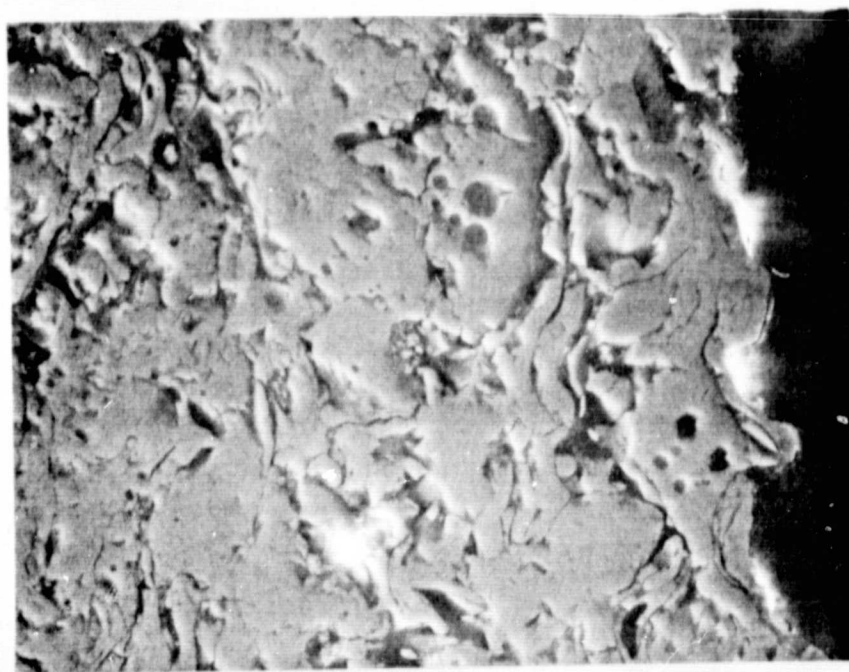
Standard
Density Layer

Porous
Oxide Layer



Magn:
100X

a. Porosity characteristics



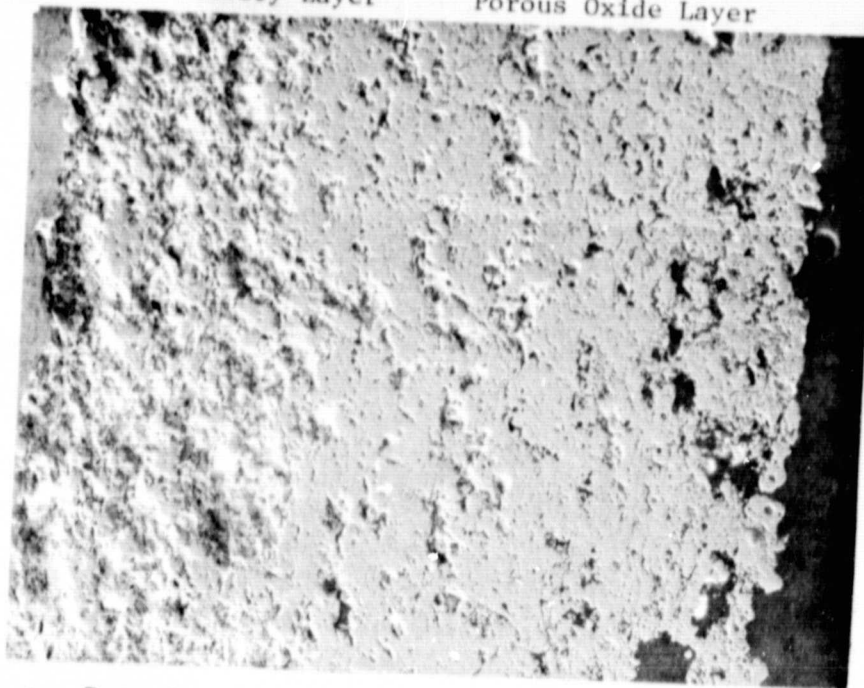
Magn:
1000X

b. Ceramic particle morphology (outer layer)

Figure 26 Porosity characteristics and ceramic particle morphology
of coating system 11-P

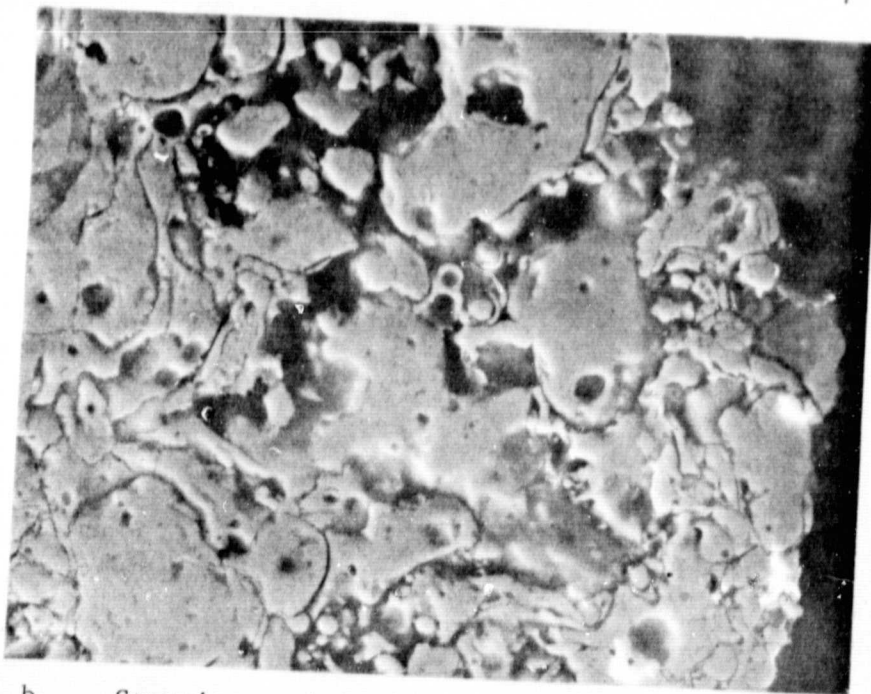
Standard Density Layer

Porous Oxide Layer



Magn:
100X

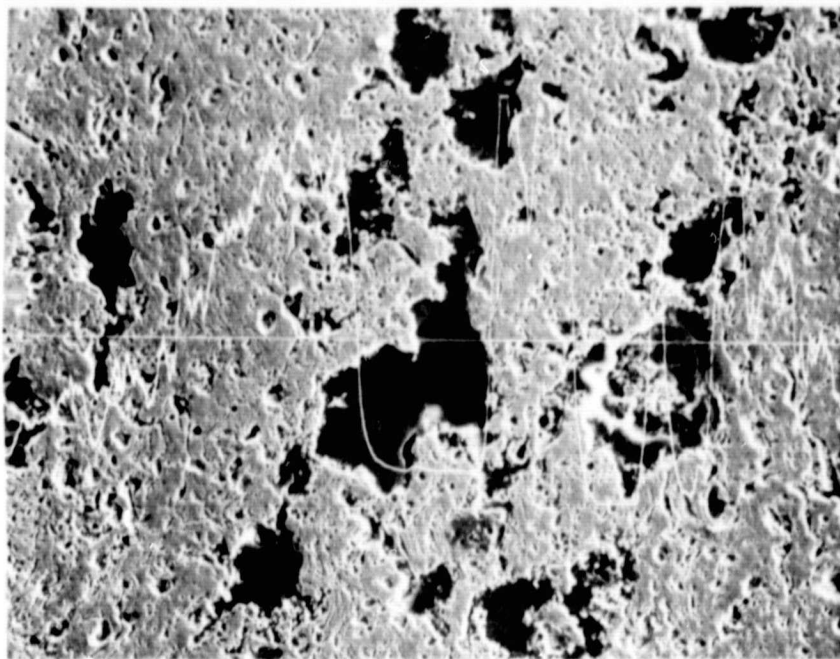
a. Porosity characteristics



Magn:
1000X

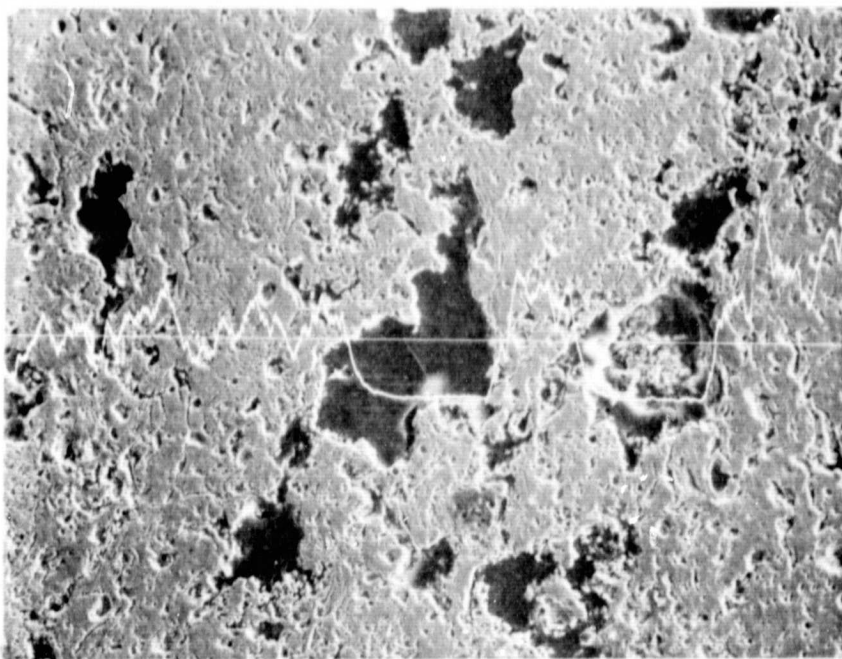
b. Ceramic particle morphology (outer layer)

Figure 27 Porosity characteristics and ceramic particle morphology of coating system III-P.



Zr scan line

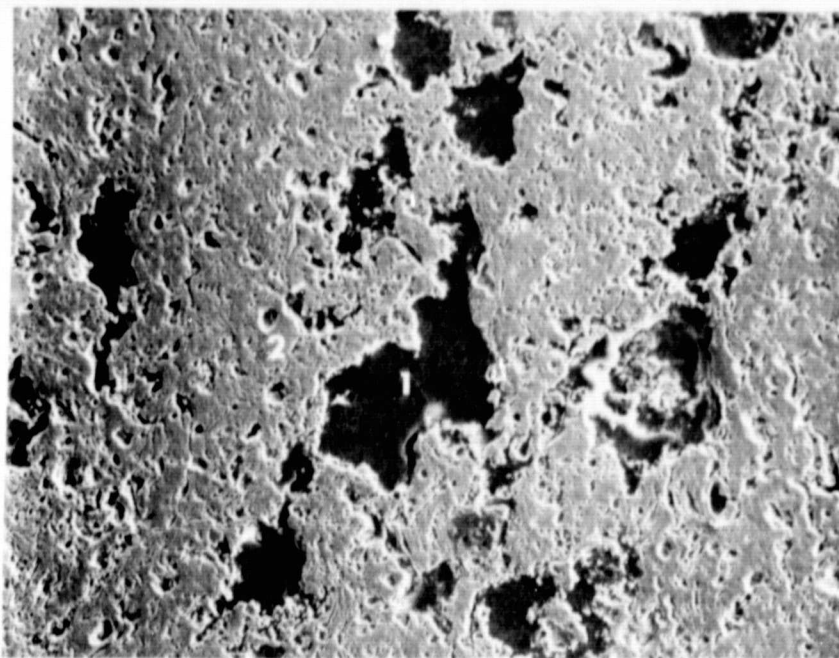
a. Elemental zirconium analysis



Y scan line

b. Elemental yttrium analysis

Figure 28 Elemental line scan analysis of coating system II-P
Magn: 200X



Mapped Zone Designation

Zone 1	Zone 2
Void area	Major: Zr Minor: Y, Hf Trace: Ca, Na, Si

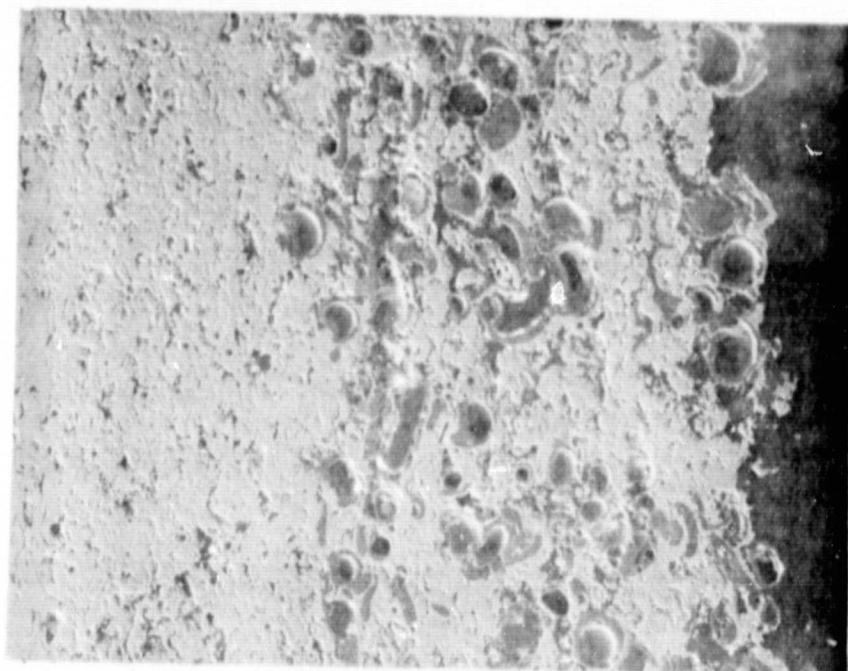
Figure 29 Mapped zones analyzed by X-ray energy dispersive analysis to identify elemental distribution in coating system IIP.
Magn: 200X

REPRODUCIBILITY OF THE
ORIGINAL PAGE IS POOR

Bond
Coat

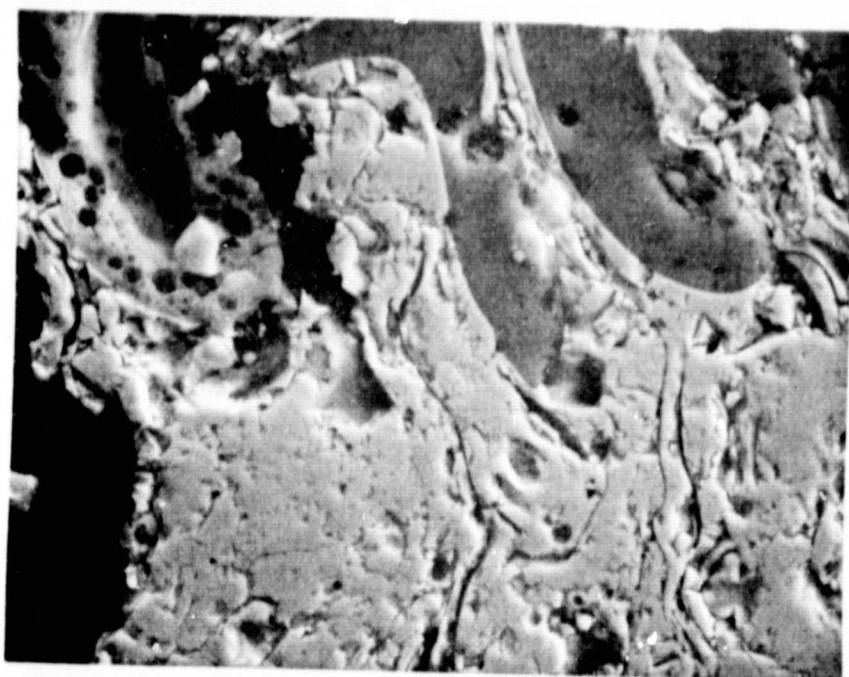
Standard Density
Layer

Filled Oxide
Layer



Magn: 100X

a. Porosity characteristics

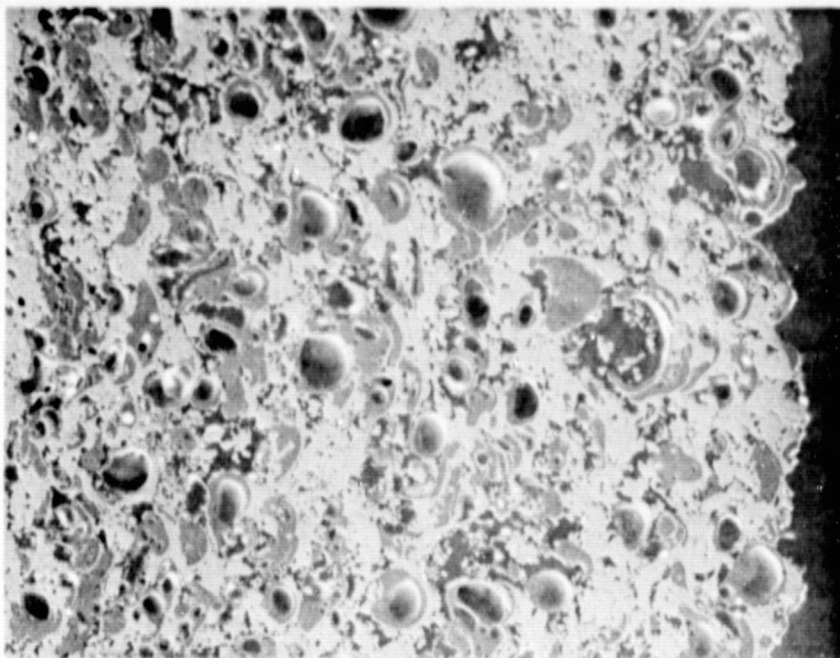


Magn: 1000X

b. Ceramic particle morphology (Outer layer)

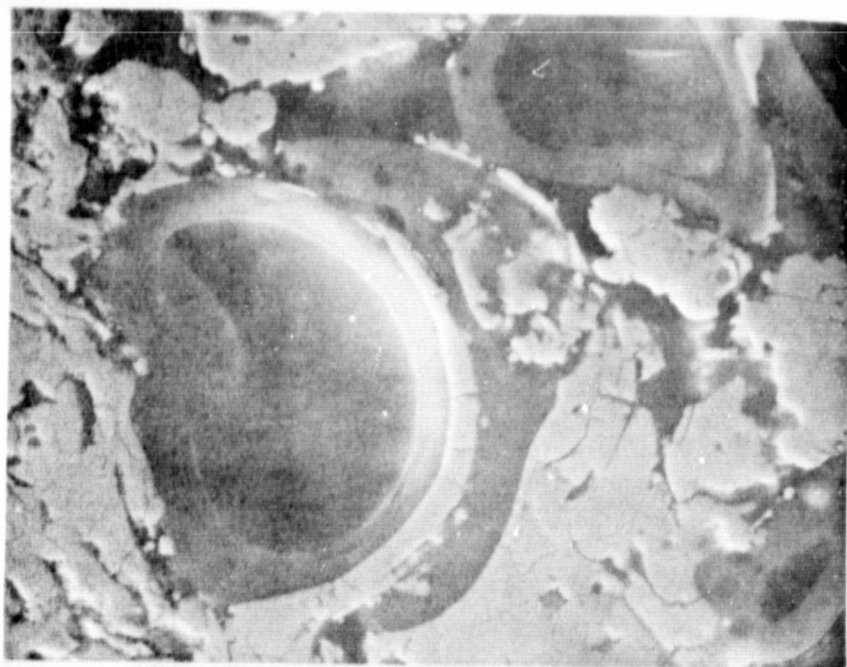
Figure 30 Porosity characteristics and ceramic particle morphology of coating system I-C

Filled Oxide Layer



Magn: 100X

a. Porosity characteristics



Magn: 1000X

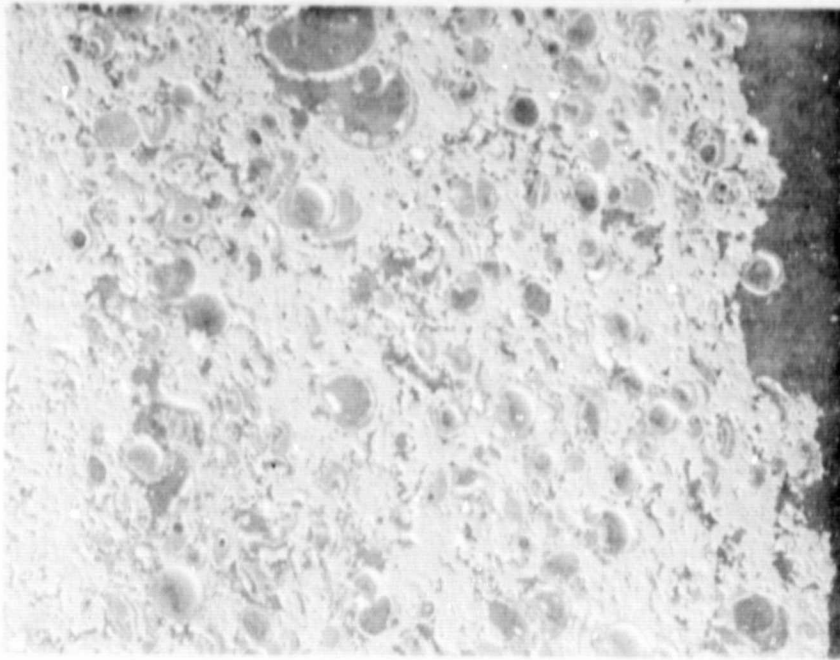
b. Ceramic particle morphology (outer layer)

Figure 31 Porosity characteristics and ceramic particle morphology of coating system II-C

REPRODUCIBILITY OF THE
ORIGINAL PAGE IS POOR

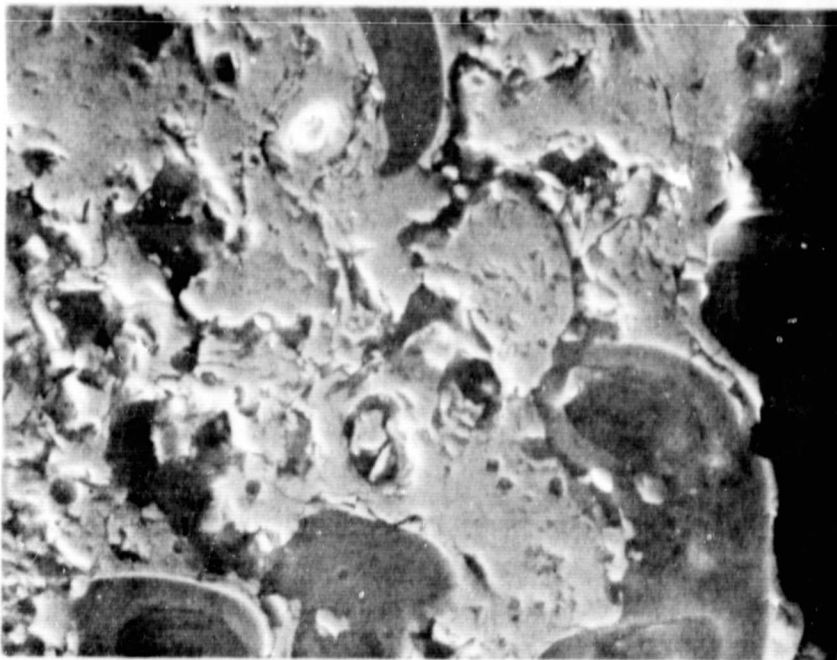
Standard
Density Layer

Filled Oxide Layer



Magn: 100X

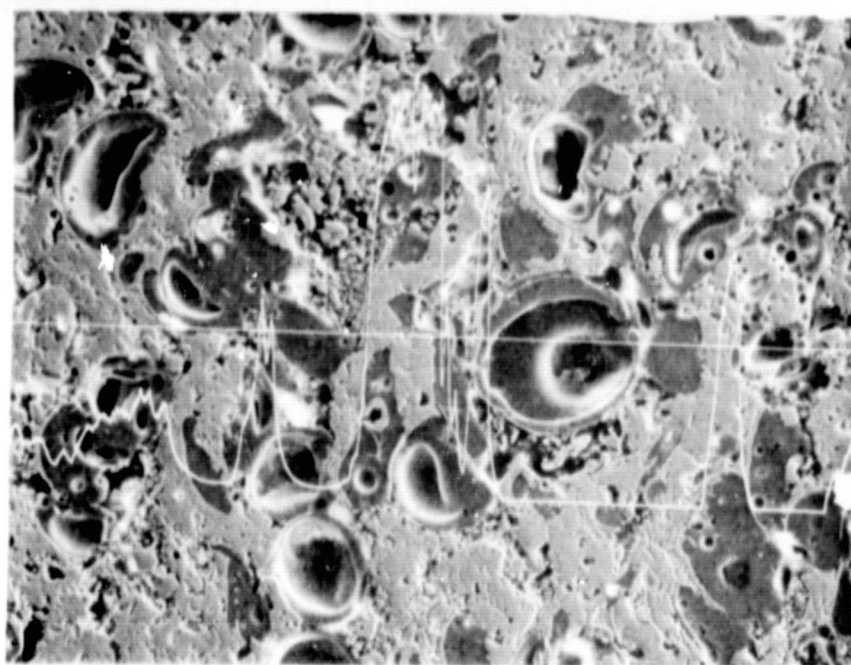
a. Porosity characteristics



Magn: 1000X

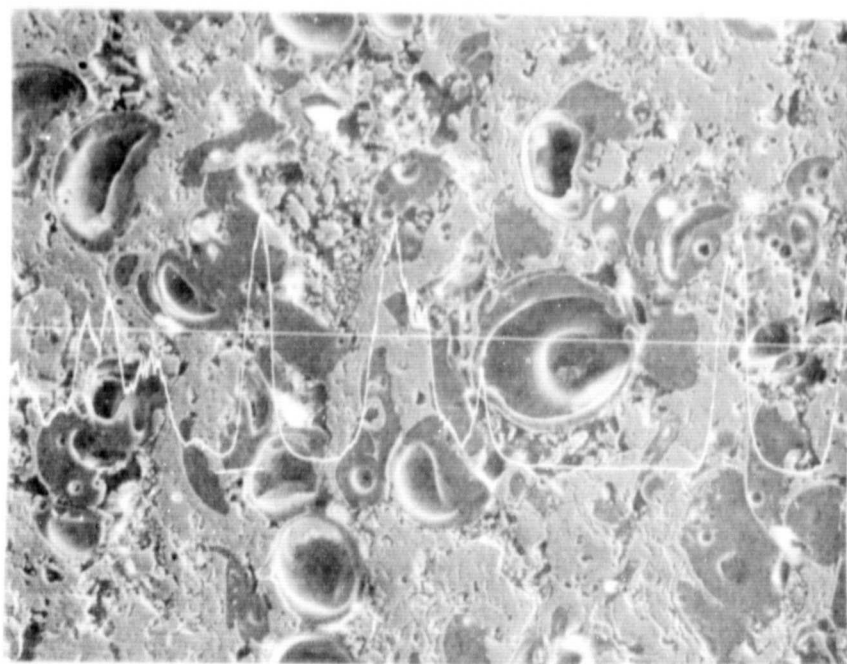
b. Ceramic particle morphology (outer layer)

Figure 32 Porosity characteristics and ceramic particle morphology of coating system III-C



Zr scan line

a. Elemental zirconium analysis

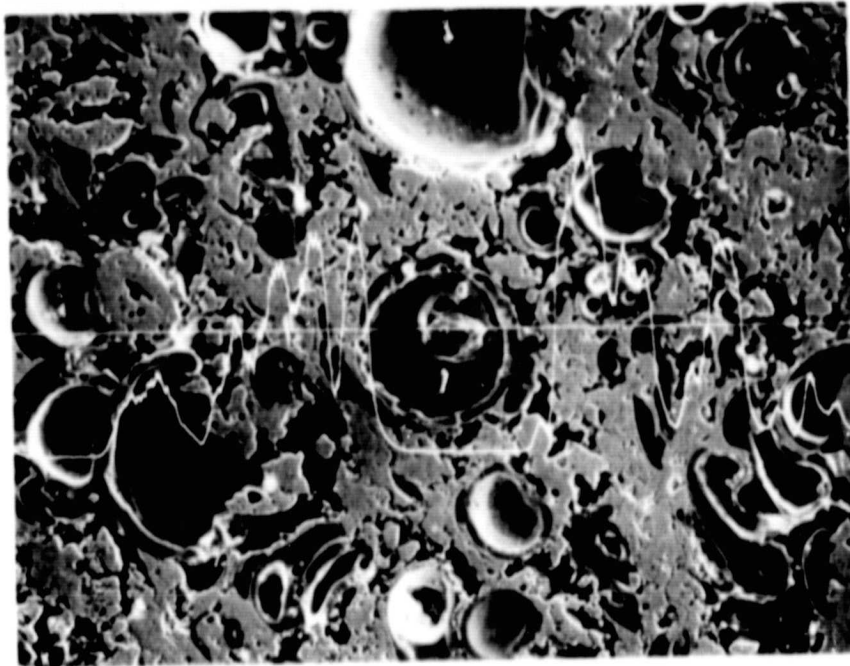


Y scan line

b. Elemental yttrium analysis

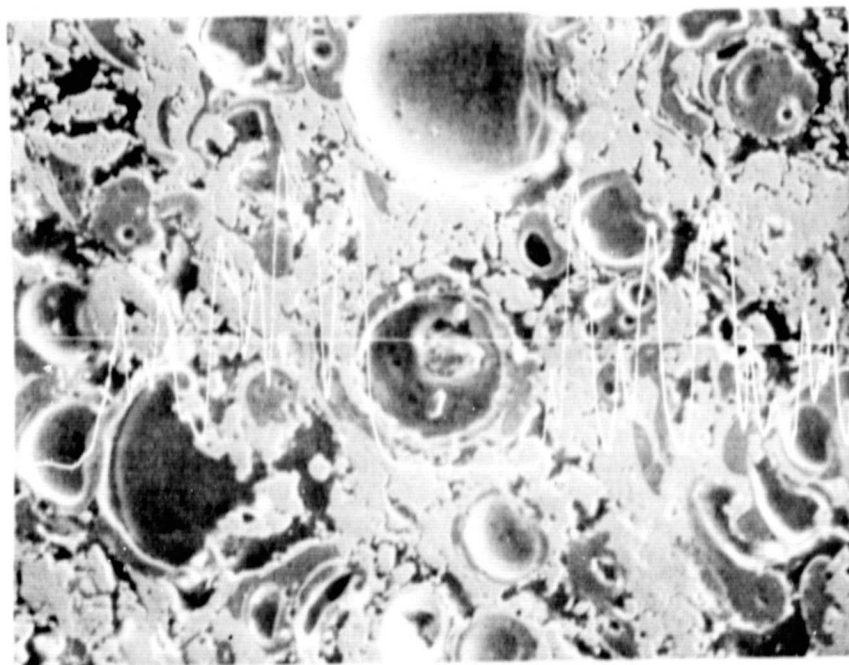
Figure 33 Elemental line scan analysis of coating system I-C Magn: 200X

REPRODUCIBILITY OF THE
ORIGINAL PAGE IS POOR



Zr scan line

a. Elemental zirconium analysis



Y scan line

b. Elemental yttrium analysis

Figure 34 Elemental line scan analysis of coating system II-C Magn: 200X